THE JOURNAL OF BIOLOGICAL CHEMISTRY VOL. 283, NO. 30, pp. 21251–21266, July 25, 2008
Printed in the U.S.A.

Characterization of Two Thermostable Cyanobacterial Phytochromes Reveals Global Movements in the Chromophore-binding Domain during Photoconversion*[S]

Received for publication, February 27, 2008, and in revised form, April 30, 2008 Published, JBC Papers in Press, May 14, 2008, DOI 10.1074/jbc.M801592200

Andrew T. Ulijasz[‡], Gabriel Cornilescu[§], David von Stetten[¶], Steve Kaminski[¶], Maria Andrea Mroginski[¶], Junrui Zhang[‡], Devaki Bhaya[‖1], Peter Hildebrandt[¶], and Richard D. Vierstra[‡2]

From the [‡]Department of Genetics and [§]National Magnetic Resonance Facility, University of Wisconsin, Madison, Wisconsin 53706, the [¶]Technische Universität, D-10623 Berlin, Germany, and the [‖]Department of Plant Biology, Carnegie Institution of Washington, Stanford, California 94305

Photointerconversion between the red light-absorbing (Pr) form and the far-red light-absorbing (Pfr) form is the central feature that allows members of the phytochrome (Phy) superfamily to act as reversible switches in light perception. Whereas the chromophore structure and surrounding binding pocket of Pr have been described, those for Pfr have remained enigmatic for various technical reasons. Here we describe a novel pair of Phys from two thermophilic cyanobacteria, *Synechococcus* sp. OS-A and OS-B′, that overcome several of these limitations. Like other cyanobacterial Phys, *SyA*-Cph1 and *SyB*-Cph1 covalently bind the bilin phycocyanobilin via their cGMP phosphodiesterase/adenyl cyclase/FhlA (GAF) domains and then assume the photointerconvertible Pr and Pfr states with absorption maxima at 630 and 704 nm, respectively. However, they are naturally missing the N-terminal Per/Arndt/Sim domain common to others in the Phy superfamily. Importantly, truncations containing only the GAF domain are monomeric, photochromic, and remarkably thermostable. Resonance Raman and NMR spectroscopy show that all four pyrrole ring nitrogens of phycocyanobilin are protonated both as Pr and following red light irradiation, indicating that the GAF domain by itself can complete the Pr to Pfr photocycle. ^{1}H-^{15}N two-dimensional NMR spectra of isotopically labeled preparations of the *SyB*-Cph1 GAF domain revealed that a number of amino acids change their environment during photoconversion of Pr to Pfr, which can be reversed by subsequent photoconversion back to Pr. Through three-dimensional NMR spectroscopy before and after light photoexcitation, it should now be possible to define the movements of the chromophore and binding pocket during photoconversion. We also generated a series of strongly red fluorescent derivatives of *SyB*-Cph1, which based on their small size and thermostability may be useful as cell biological reporters.

Phytochromes (Phys)[3] include a large and diverse superfamily of sensory photoreceptors that use a bilin (or linear tetrapyrrole) chromophore for light detection (1–3). These chromoproteins were first discovered in higher plants based on their control of many agriculturally relevant processes and have since been found by sequence searches in lower plants, algae, and numerous proteobacteria, cyanobacteria, and fungi. For photoautotrophic organisms, Phys are particularly important for optimizing photosynthetic potential where they measure the fluence rate, duration, and the direction of light and help detect shading by competitors (1, 4).

The signature feature of canonical Phys is their ability to photoconvert between two stable states, a red light-absorbing Pr form that is typically the parent state of the photoreceptor, and a far-red light-absorbing Pfr form that is often biologically active (1–3) (for examples of exceptions see Refs. 5–7). This activity is directed by a series of structural domains that play specific roles in photoperception. A large N-terminal region encompasses the chromophore-binding domain (CBD); it includes a proximal Per/Arndt/Sim (PAS) domain immediately followed by a cGMP phosphodiesterase/adenyl cyclase/FhlA (GAF) domain. The CBD autocatalytically attaches the bilin via a thioether linkage and together with the chromophore generates the unique photochromic absorption properties of Phys.

For proteobacterial (BphP) and fungal Phys, biliverdin (BV) is used as the chromophore (8). BV is synthesized by oxidative cleavage of heme by a heme oxygenase (HO) and then attached to the apoprotein through its A-pyrrole ring vinyl side chain to a positionally conserved cysteine upstream of the PAS domain (9, 10). For cyanobacterial (Cph) and plant Phys, phycocyanobilin (PCB) and phytochromobilin (PΦB) are used as the chromophore, respectively (2, 11, 12). PCB/PΦB are synthesized by enzymatic reduction of BV using a BV reductase (BVR) and then attached through their A-ring ethylidene side chains to a

* This work was supported in part by National Science Foundation Grants MCB 0424062 and 07191530 (to R. D. V.), Deutsche Forschungsgemeinschaft Grant SF498 (to P. H. and M. A. M.), and an American Heart Association postdoctoral fellowship (to A. T. U.). The costs of publication of this article were defrayed in part by the payment of page charges. This article must therefore be hereby marked "*advertisement*" in accordance with 18 U.S.C. Section 1734 solely to indicate this fact.

[S] The on-line version of this article (available at http://www.jbc.org) contains supplemental Figs. 1–5.

[1] Supported by the National Science Foundation and the Carnegie Institution of Washington.

[2] To whom correspondences should be addressed: Dept. of Genetics, 425-G Henry Mall, University of Wisconsin, Madison, WI 53706. Tel.: 608-262-8215; Fax: 608-262-2976; E-mail: vierstra@wisc.edu.

[3] The abbreviations used are: Phy, phytochrome; BphP, bacteriophytochrome; BV, biliverdin IXα; CBD, chromophore-binding domain; Cph, cyanobacterial phytochrome; GAF, cGMP phosphodiesterase/adenyl cyclase/FhlA; HK, histidine kinase; HO, heme oxygenase; HSQC, heteronuclear single quantum coherence; PAS, Per/Arndt/Sim; PCB, phycocyanobilin; PΦB, phytochromobilin; PHY, phytochrome domain; Pr, red light-absorbing form of phytochrome; Pfr, far-red light-absorbing form of phytochrome; RR, resonance Raman; *SyA/B*, *Synechoccous* sp. OS-A/OS-B′; *Syn*, *Synechocystis*; BVR, BV reductase; FPLC, fast protein liquid chromatography; ALA, α-aminolevulinic acid; SEC, size exclusion chromatography.

positionally conserved cysteine in the GAF domain. Despite these differences in binding geometry, it appears that the positioning of the bilin in the CBD is similar in both the BV- and PCB/PΦB-containing Phys (13). Following the GAF domain is a phytochrome (PHY) domain that helps stabilize the Pfr form (14, 15).

The C-terminal half of Phys contains one or more domains that promote signal output. The most common in microorganisms is a histidine kinase (HK) domain that allows Phys to participate in specific two-component signal transduction cascades (3). Higher plant Phys have C-terminal sequences related to HK domains (2, 3), but it has not yet been confirmed that they function as protein kinases.

Despite intensive effort, it still remains unclear how Phys photointerconvert between Pr and Pfr and how this change initiates signal transmission (2). Important insights were provided recently by determinations of the three-dimensional structure of the CBD as Pr. These high resolution x-ray crystallographic models, which were generated with proteobacterial Phys from *Deinococcus radiodurans* (*Dr*BphP) (10, 13) and *Rhodopseudomonas palustris* BphP3 (53) assembled with BV, revealed that that the bilin is deeply buried within the GAF domain in a *ZZZ-syn,syn,anti* configuration. The PAS domain has no direct contact with the chromophore; instead, it is connected indirectly to the bilin and the GAF domain through a figure-of-eight knot in the polypeptide. These models also identified a number of amino acid contacts potentially important for bilin binding and photochemistry that we and others have confirmed to be critical by mutagenic analysis of recombinant chromoproteins (13, 15–19). For example, the aspartate residue (Asp-207 in *Dr*BphP) within an invariant Asp-Ile-Pro (DIP) motif was shown to be essential for photoconversion, presumably by helping coordinate a fixed water (pyrrole water) adjacent to the pyrrole nitrogens of rings A–C (18, 19).

In contrast to our detailed understandings of Pr, we know little about the structure of Pfr. A variety of spectroscopic studies has proposed that Pr → Pfr phototransformation first involves a *Z* to *E* isomerization of the methine bridge double bond between the C and D pyrrole rings to form the Lumi-R intermediate (20–22). The transition from Lumi-R to Pfr then proceeds by a series of relaxation steps that include deprotonation/reprotonation of the pyrrole ring nitrogens (23, 24) along with conformational changes within the protein, which ultimately affect the C-terminal output domain. Although the environment of several regions of the polypeptide have been indirectly shown to change during photoconversion (*e.g.* (25–31)), the extent of the conformation movements is not yet clear.

To help resolve the structure of Pfr, we and others (32–34) have begun to explore NMR spectroscopic approaches to determine its solution structure. Here we describe a pair of Cphs from two *Synechococcus* strains (designated *SyA*-Cph1 and *SyB*-Cph1) that offer several advantages. One useful feature is their remarkable stability across a wide range of temperatures, which enhances their survival during NMR data collection. Another was revealed from sequence alignments, which showed that they are members of a previously uncharacterized subfamily of Phys that lacks the N-terminal PAS domain, previously considered important for holo-protein assembly and photochromicity (2, 3). Truncations containing just the ~200-amino acid GAF domain are photoactive, thus placing them within the acceptable size range for NMR studies (35, 36). Remarkably, two-dimensional ^{1}H-^{15}N heteronuclear single quantum coherence (HSQC) NMR spectra of the *SyB*-Cph1(GAF) truncation collected before and after red light irradiation detected changes for numerous amide nitrogens, suggesting that the GAF domain changes conformation more substantially during Pr → Pfr photoconversion than anticipated. We also engineered a set of GAF domain mutants in *SyB*-Cph1 that are strongly red fluorescent, which may have use as cell biological reporters.

EXPERIMENTAL PROCEDURES

Operon Organization and Sequence Alignment—Genomic sequences for the *SyA-Cph1* and *SyB-Cph1* operons from *Synechococcus* sp. OS-A (also referred to as sp. JA-3–3Ab: NCBI accession NC_007775) and *Synechococcus* sp. OS-B′ (also referred to as sp. JA-2–3B′a(2-13): NCBI accession number NC_007776) were obtained from The Institute for Genomic Research (TIGR) comprehensive microbial resource (CMR) website. Operon organizations were predicted by the FGENESB bacterial and operon gene prediction and TIGR CMR operon prediction functions. Related proteins were identified by BLAST searches of the GenBank™ data base (www.ncbi.nlm.nih.gov), aligned by ClustalW, and displayed using MACBOXSHADE version 2.18 (Institute of Animal Health, Pirbright, UK).

Construction of Recombinant Phy Expression Strains—PCR-based modifications of Phys involved paired amplifications that were subsequently combined, melted, and re-annealed to generate blunt-ended doubled-stranded fragments as described (37). The DNA templates for *SyA-Cph1* and *SyB-Cph1* full-length coding sequences were PCR-amplified directly from *Synechococcus* sp. OS-A and OS-B′ genomic DNA, respectively. The pBAD-C expression plasmid encoding the PAS-GAF-PHY region from *Synechocystis* sp. PCC6803 (*Syn*) Cph1 (residues 1–514) was as described (38). The codons for the C-terminal c-Myc tag attached to *Syn*-Cph1(PAS-GAF-PHY) were replaced with those encoding a His_6 tag (underlined) followed by a stop codon by ligating the annealed primers 5′-AGCTTTGCATCATCAT-CATCATCATTGAAGC and 5′-AGCTGCTTC-AATGATGATGATGATGATGCAA into HindIII-digested pBAD-C plasmid containing the *Syn*-Cph1(PAS-GAF-PHY) construction. From this manipulation, the plasmid pBAD-6H was generated.

Assembly of the various Cph truncations and mutants were accomplished by PCR using appropriate primer pairs. Products for the two PCRs were combined, melted, and re-annealed, phosphorylated, and purified as described (37). Phosphorylated flush inserts were then ligated into the NcoI- and HindIII-digested pBAD-6H plasmid. Site-directed mutations were introduced into the His_6-tagged *SyB*-Cph1(GAF) construction by the QuickChange method (Stratagene, La Jolla, CA) using *Pfx* polymerase (Invitrogen) in combination with the appropriate mutagenic primers. All coding regions were sequenced in their entirety to confirm the presence of the desired mutation and the absence of secondary mutations.

The PAS-GAF-PHY truncation (residues 1–501) of *Dr*BphP was generated by PCR amplification of the full-length coding region with the primers 5′-CGTAAGGATCCATGAGCCGGGACCCGTTGCCC and 5′-CCTGACTCGAGCGCCCCGGTCAATGTGTCACG that were designed to add BamHI and XhoI sites to the 5′ and 3′ ends, respectively. The PCR product was digested with BamHI and XhoI and ligated into the pET21a plasmid (Novagen, Madison, WI) that was similarly digested.

Protein Expression and Purification—PCB-containing holo-Cphs suitable for absorption, resonance Raman (RR), and/or NMR spectroscopy were produced using a dual-plasmid *Escherichia coli* expression system (38). The kanamycin resistance plasmid pPL-PCB expressed the HO and BVR enzymes under isopropyl 1-thio-β-D-galactopyranoside control to direct the synthesis of PCB from heme. Ampicillin resistance pBAD-6H plasmids expressed the His_6-tagged *SyA*-Cph1, *SyB*-Cph1, and *Syn*-Cph1 truncations solely under arabinose control (38). The pPL-PCB and pBAD-6H plasmids were simultaneously introduced into the *ara* operon-deficient *E. coli* expression strain BL21-AI (Invitrogen) and cultured in 500 ml of repression medium (RM (38)) to suppress protein production. After an overnight incubation, the cells were harvested, resuspended, and grown at 37 °C in 2 liters of M9 minimal medium containing NH_4Cl, 0.2% glycerol, 100 μM α-aminolevulinic acid (ALA) (39), 100 μM $FeCl_3$, 5 mg of thiamine, and a vitamin mix (40). To synthesize isotopically labeled *SyB*-Cph1(GAF), NH_4Cl and glycerol were replaced with ^{15}N- and ^{13}C-isotopically labeled forms, respectively. To produce *SyB*-Cph1(GAF) that contained either [^{15}N]PCB or [^{13}C]PCB (isotopically labeled at all six methyl groups and the $C8^2$ and $C12^2$ methylene carbons (see Fig. 8*A*)) attached to unlabeled protein, unlabeled ALA in the medium was replaced with 100 μM [^{15}N]ALA (Medical Isotopes Inc., Pelham, NH) or 1,2-[^{13}C]ALA (a gift from Dr. Mario Rivera, Kansas State University), respectively. In all cases, once the A_{600} of the culture reached 0.8–0.9, PCB synthesis was induced by adding 1 mM isopropyl 1-thio-β-D-galactopyranoside. After 2 h, synthesis of the Cph1 apoproteins was induced by the addition of 0.2% w/v arabinose, and the cultures were grown overnight at 20 °C. All subsequent steps were performed under dim green light.

To purify the various Phy chromoproteins, the expressing cells were collected by centrifugation, resuspended in 25 ml/liter of culture in lysis buffer (50 mM Tris-HCl (pH 8.0), 100 mM NaCl, 1 mM dithiothreitol, 1 mM phenylmethylsulfonyl fluoride, and a tablet of Complete-EDTA free protease inhibitor mixture (Hoffmann-La Roche)), and lysed by sonication. Nonidet P-40 (0.1% v/v) was then added to the lysates followed by incubation on ice for 30 min, agitation at 4 °C for 2 h, and finally clarified by centrifugation at 16,000 × *g* for 30 min. The resulting supernatant was filtered through a 0.45 μm filter (Corning Glass) and dialyzed into wash buffer (50 mM Tris-HCl (pH 7.0), 300 mM NaCl, 10% (v/v) glycerol, 20 mM imidazole, 0.05% (v/v) Tween 20, and 1 mM 2-mercaptoethanol) overnight at 4 °C as described (38). The Phy chromoproteins were then purified by nickel chelate-affinity chromatography (Qiagen Sciences, Germantown, MD) using the wash buffer plus 300 mM imidazole for elution. The Phy-containing eluates were then subjected to hydrophobic interaction FPLC using a 1 × 10-cm phenyl-HP column (GE Healthcare) with a 0–300 mM ammonium sulfate gradient in 25 mM Tris-HCl (pH 8.0) for elution. Pooled Phy-containing fractions for NMR analysis were exchanged and concentrated into 10 mM deuterated Tris-HCl (pH 8.5) (Sigma) in 100% H_2O using an Amicon Ultra-15 filter (Millipore, Billerica, MA). [^{13}C]PCB containing samples were exchanged into 10 mM Tris-DCl (pH 8.5) in 100% D_2O. This buffer was found to enhance the stability of *SyB*-Cph1(GAF) chromoprotein based on the solubility screen of Collins *et al.* (41). For all nonisotopically labeled Cph1 holo-proteins, the same protocol was applied except nonisotopically labeled reagents were used in the M9 medium preparation, and the FPLC purification step was omitted.

To test for bilin specificity, the various Phy apoproteins were expressed in the pBAD-6H plasmid as above without co-expression of the *HO* and *BVR* genes from pL-PCB. Apo-*Dr*BphP-(PAS-GAF-PHY) C-terminally tagged with a His_6 sequence was expressed as described by Karniol *et al.* (15). The *E. coli* cells were resuspended in 30 mM Tris-HCl (pH 8.0), 100 mM NaCl, and 30 mM imidazole and lysed by sonication. The resulting extracts were clarified by centrifugation as above and then mixed with 100 μM of either PCB or BV for 2 h at 4 °C. The polypeptides were purified by nickel-chelate affinity chromatography using 300 mM imidazole for elution. Presence of the covalently bound bilin was assayed by zinc-induced fluorescence of the chromoproteins following SDS-PAGE (8). PCB was purified from lyophilized *Spirulina platensis* as described (42) but without the final high pressure liquid chromatography step. Purified BV was obtained from Frontier Scientific (Logan, UT).

Size Exclusion Chromatography—Size exclusion chromatography (SEC) was performed by FPLC using a 24-ml Superose 6 (S6) column (GE Healthcare). The chromoproteins (100 μl of a 5 mg/ml sample) were first purified through the phenyl-HP step, dissolved in 30 mM Tris-HCl (pH 8.0) and 200 mM NaCl, and either loaded onto the column as Pr or immediately following saturating irradiation of the samples with red light (620 nm). Absorption spectra were recorded before and after SEC to verify that the chromoproteins remained enriched in the desired states (Pr or Pfr).

Absorption and Fluorescence Spectroscopy—Absorption spectra were measured with a Lambda 650 UV-visible spectrophotometer (PerkinElmer Life Sciences) with the samples dissolved in 30 mM Tris-HCl (pH 8.0). Photoconversions between Pr and Pfr by red and far-red light were achieved with white light filtered through appropriate interference filters (10 nm half-bandwidth) (Andover Corp., Salem, NH), 620-nm and 690-nm filters, respectively, for *SyA*-Cph1 and *SyB*-Cph1, and 660-nm and 774-nm filters, respectively, for *Syn*-Cph1. Thermostability was measured in the dark for Pr samples (absorbance of the Pr absorption maximum was adjusted to 1.5) dissolved in 30 mM Tris-HCl (pH 8.0). After heating for 20 min at the appropriate temperature, the samples were clarified by centrifugation at 16,000 × *g*, and the amounts of soluble chromoproteins remaining were measured spectrophotometrically. Rates of Pr → Pfr photoconversion and Pfr → Pr dark reversion were measured using the absorbance of the samples at 704 nm to determine the amount of Pfr generated or lost, respectively.

Fluorescence excitation and emission spectra were recorded with a QuantaMaster model C-60/2000 spectrofluorimeter (Photon Technologies International, Birmingham, NJ). Chromoprotein concentrations were adjusted to have an absorbance of 0.6 for the Pr absorbance maximum. Emission spectra were recorded during an excitation at 360 nm. Excitation spectra were recorded by measuring fluorescence at the peak emission wavelength (646–664 nm depending on the sample).

RR Spectroscopy—RR spectra were recorded with 1064-nm excitation (Nd-YAG cw laser, line width <1 cm^{-1}) using Digilab (Bio-Rad) or an RFS 100/S (Bruker Optics, Ettlinger, Germany) Fourier-transform Raman spectrometer (4 cm^{-1} spectral resolution). The near-infrared excitation line was sufficiently close to the first electronic transition to generate a strong pre-resonance enhancement of the chromophoric vibrational bands such that Raman bands of the protein matrix remained very weak in the spectra of the parent states (18, 43). All spectra were measured at −140 °C using a liquid nitrogen-cooled cryostat (Linkam, Waterfield, Surrey, UK). The laser power at the sample was set at ~700 milliwatts, which did not damage the chromoproteins as checked by comparing the absorption spectra of the samples obtained before and after RR data acquisition. The total accumulation time was less than 2 h for each spectrum. For all RR spectra shown in this work, the background was subtracted.

To detect photoproducts that accumulate in red light, the samples were irradiated at room temperature and then rapidly frozen to liquid nitrogen temperatures. The raw RR spectra included substantial contributions from residual Pr, which was subtracted using the characteristic RR bands of Pr as a reference. Further RR experimental details have been described previously (18, 19, 43).

NMR Spectroscopy—Isotopically labeled forms of *SyB*-Cph1(GAF) assembled with PCB (~2 mM) were dissolved in 93% H_2O, 7% D_2O, 10 mM deuterated Tris-HCl (pH 8.5), and 0.15 mM NaN_3 and placed in a 280-μl Shigemi microcell. Prior to NMR analysis, the tube was heated to 65 °C for 10 min to inactivate contaminating thermosensitive *E. coli* proteases that slowly compromised the sample (data not shown). NMR spectra were collected at 25 °C using an 800-MHz ^{1}H frequency Varian INOVA spectrometer (Varian Inc., Palo Alto, CA) equipped with a cryogenic probe. Samples with a high proportion of Pfr were obtained by irradiating the microcell solution with saturating red light (620 nm); this photoequilibrium was maintained throughout NMR data acquisition by continuous irradiation of the microcell with a low fluence rate of red light provided by a 1-watt, 620-nm light-emitting diode (LED) (LiteON LED, Mouser Electronics, Mansfield, TX) channeled into the glass plunger by a fiber optic cable. This irradiation scheme maintained ~50% of the chromoprotein in the Pfr form, based on comparisons of NMR peak intensities throughout data acquisition. Photoconversion of Pfr back to Pr was completed by irradiating the microcell with saturating far-red light (690 nm).

^{1}H-^{15}N HSQC spectra with ^{15}N-^{13}C-labeled *SyB*-Cph1(GAF) chromoprotein or unlabeled *SyB*-Cph1(GAF) protein assembled with [^{15}N]PCB were collected as 128* (t_1, ^{15}N) × 1022* (t_2, ^{1}H) data matrices. Acquisition times were 48 and 85 ms in the t_1 and t_2 dimensions, respectively. ^{1}H-^{13}C HSQC spectra that centered on the methyl region of unlabeled *SyB*-Cph1(GAF) protein assembled with [^{13}C]PCB were collected as 32*(t_1, ^{13}C) × 769* (t_2, ^{1}H) data matrices. Acquisition times were 10 and 80 ms in the t_1 and t_2 dimensions, respectively. Data were processed and plotted using the NMRPipe software package (44). All NMR data were collected at the National Institutes of Health-sponsored NMR Facility at the University of Wisconsin, Madison.

RESULTS

SyA-Cph1 and SyB-Cph1 Identify a New Subfamily of Phys—During our continued effort to determine the breadth of microorganisms containing Phys (15) and to identify Phys with novel structures and/or photochemical properties (5–7), we discovered a potentially useful collection from a metagenomics project aimed at cataloging microbial communities within Yellowstone National Park hot springs (45, 46). The DNA sequences originated from two newly described cyanobacterial species designated *Synechococcus* sp. Octopus Spring (OS)-A and OS-B′, which based on the optimal growth temperature of the organisms would likely encode thermostable Phy-type photoreceptors. Included were possible orthologs of *Synechocystis* (abbreviated as *Syn*) Cph2 (14, 47) and TaxD1/PixJ (48, 49), suggesting that these cyanobacteria employ an array of bilin-containing photoreceptors for their light behaviors (50).

For our goals, the most relevant were two *Phy* genes, designated here as *SyA-Cph1* (TIGR locus number CYA_2779) and *SyB-Cph1* (TIGR locus number CYB_2465), that encode proteins with obvious GAF and PHY domains near their N termini (Fig. 1). Each of the GAF domains includes the following. (i) The positionally conserved cysteine (Cys-138 in *SyB*-Cph1) used by Cphs to covalently bind PCB (12, 51). (ii) The conserved aspartic acid (Asp-86 in *SyB*-Cph1) within the invariant DIP motif that helps coordinate the pyrrole water associated with the bilin (13). (iii) A set of conserved/similar residues within the GAF domain that have been shown to be important for bilin ligation (*e.g.* Arg-133, His-139, and His-169 in *SyB*-Cph1) and Pr → Pfr phototransformation (*e.g.* Tyr-54, Asp-86, Phe-82, Phe-95, Tyr-142, and His-169 in *SyB*-Cph1) in other Phys (13, 16–19, 52). Taken together, it was highly likely that these Cphs assemble with linear bilins and become red/far-red photochromic.

A novel structural feature that is most likely common to the CBD of canonical Phys is a figure-of-eight knot that helps tether the PAS and GAF domains (10, 13, 53). The ~33-amino acid loop sequence that forms the knot lasso is present within the GAF domains of both *SyA*-Cph1 and *SyB*-Cph1 (Fig. 1*B*). Likewise, amino acid sequence alignments revealed strong conservation within the PHY domains of both photoreceptors (Fig. 1*B*). Obvious HK domains are also present at their C termini (supplemental Fig. 1). Included within the HK sequence are recognizable H, N, D/F, and G boxes present in typical HKs, with the H box containing the positionally conserved histidine (His-608) expected to participate in phosphotransfer (8, 12, 54, 76).

The most striking feature of the *SyA*-Cph1 and *SyB*-Cph1 sequences is the clear absence of the N-terminal PAS domain (Fig. 1), an unusual architecture first found with *Syn*-Cph2 (14,

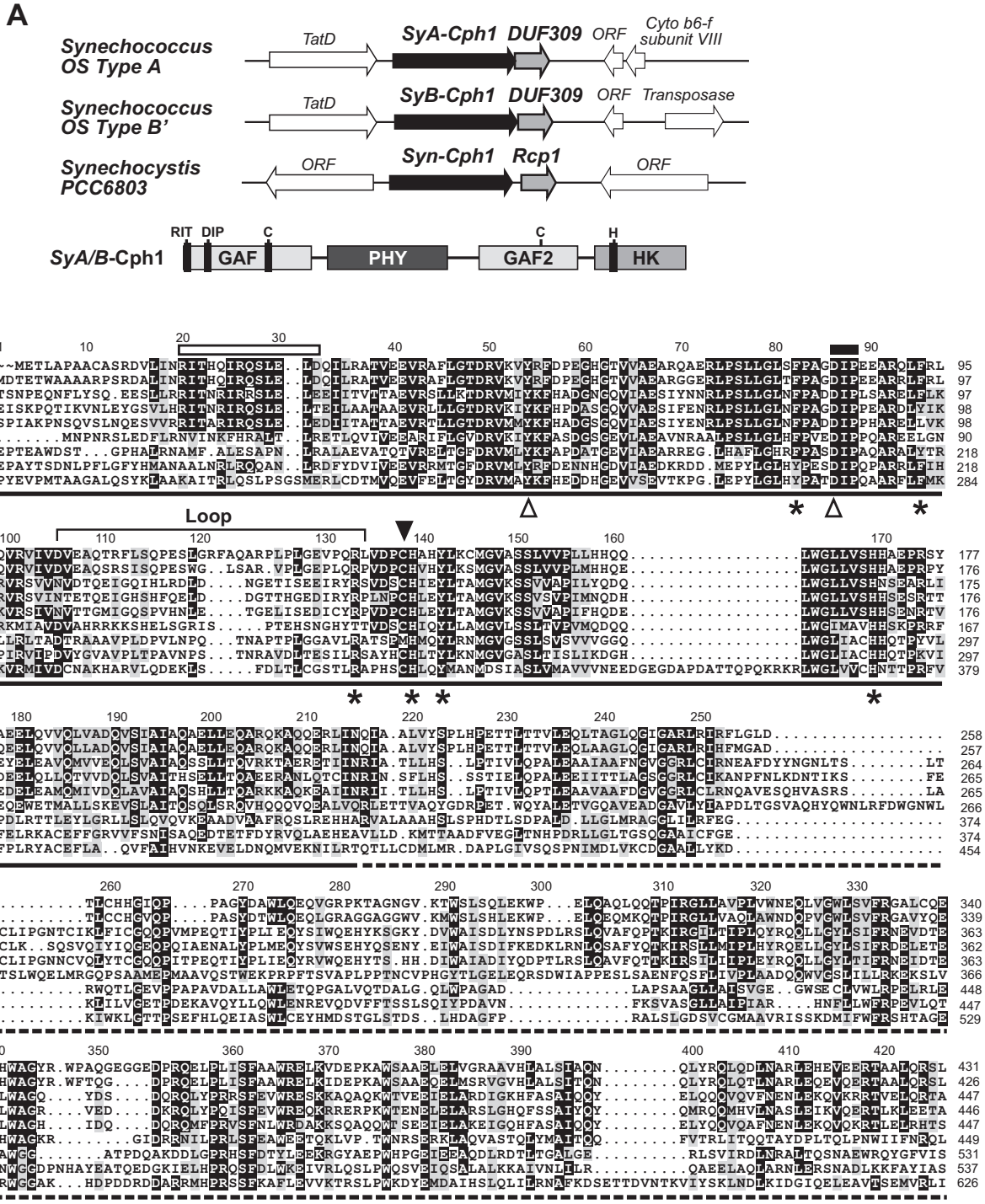

FIGURE 1. **Organization of the *SyA*-Cph1 and *SyB*-Cph1 operons and proteins from *Synechococcus* sp. OS-A and OS-B'.** *A,* diagrams of the operons and domain architectures of the encoded proteins. The *Syn*-Cph1 operon from *Synechocystis* sp. PCC6803 is included for comparison. Cph1 coding regions are shown in *black boxes*. Other coding regions within the operons and nearby separate genes are shown in *gray* and *white boxes*, respectively. Positions of the conserved RIT and DIP motifs, the GAF cysteine (*C*) that binds PCB, the conserved cysteine in GAF2, and the conserved histidine (*H*) that is the likely phosphoacceptor site in the HK domain are indicated. *ORF*, open reading frame. *B,* alignment of GAF-PHY modules in *SyA*-Cph1 and *SyB*-Cph1 with representatives from the Phy superfamily. Identical and similar amino acids are shown in *black* and *gray boxes*, respectively. *Dots* denote gaps. The RIT and DIP motifs are indicated by *open* and *black rectangles*, respectively, and the PCB-binding cysteine by the *arrowhead*. *Asterisks* identify conserved amino acids shown to be photochemically important in other Phys (16–19). The GAF lasso loop sequence that forms part of the figure-of-eight knot in *Dr*BphP (10) is defined by the *bracket*. The GAF and PHY domains are shown by the *solid* and *dashed lines*, respectively. Sequences in the alignment include those from *SyA*-Cph1 (YP_476144), *SyB*-Cph1 (YP_478662), related Cphs from *N. punctiforme* PCC73102 (ZP_00111485), *Lyngbya* sp. PCC8106 (ZP_01618934), *A. variabilis* (YP_324761), *D. radiodurans DrBphP* (INP_285374), *Synechocystis* sp. PCC6803 Cph1 (NP_442237), and Cph2 (BAA10536), and *Arabidopsis thaliana* PhyA (AAC33219). The amino acid numbering is based on the *SyB*-Cph1 sequence.

47). Although the contribution(s) of the PAS domain to Phy function are not yet clear, crystal structures reveal that it is in loose contact with the GAF domain through electrostatic interactions between the knot interface and the propionate side

chain of the B pyrrole ring (10, 53). Additional BLAST searches of the GenBank™ data base revealed a small collection of related Cphs also beginning with the GAF domain, including sequences from the mesophilic *Nostoc punctiforme, Lyngbya*, *Anabaena variabilis*, and *Acaryochloris marina* species (Fig. 1*B*, supplemental Fig. 2, and data not shown). Like *Syn*-Cph2, this new subfamily of "PAS-less" Phys contain one or two additional GAF domains downstream of the PHY domain (Fig. 1*A* and supplemental Fig. 2). The GAF2 sequences lack the DIP motif, the lasso loop sequence, and a number of other conserved residues present in the canonical GAF domain of Phys (see above), but they do contain a cysteine (Cys-516 in *SyB*-Cph1) within a Cys-His-Leu motif that could interact with bilins covalently (supplemental Figs. 1 and 2).

Although related to *Syn*-Cph2, this PAS-less Phy family was easily distinguished by the presence of a C-terminal HK domain and a signature 12-amino acid sequence RIT*X*(Q/R)IR(Q/R)SLEL or RIT motif (where *X* is any amino acid) at the N-terminal end of the first GAF domain (residues 20–31 in *SyB*-Cph1 (Fig. 1*B*)). The function of the RIT motif is unclear. The corresponding stretch in the *Dr*BphP CBD structure forms the α4-helix and α4-α5-helix linker domain, which includes part of the three-helix bundle that may help sister GAF domains dimerize (13).

Analysis of the surrounding genomic region revealed that the *SyA-Cph1* and *SyB-Cph1* coding regions are the first part of a two-locus operon in *Synechococcus* sp. OS-A and OS-B′ (Fig. 1*A*). The immediate 3′ open reading frames (TIGR locus numbers CYA_2781 and CYA_2484), which are 4-bp downstream or overlap with the *Cph1* coding region, respectively, encode small (130 residues in OS-A and 123 residues in OS-B′), highly conserved proteins predicted to contain a domain of unknown function 309 (DUF309). This domain can be found in a number of archaeal, bacterial, fungal, algal, and higher plant species where it may bind metals via the consensus H*XXXEXX*(W/Y) sequence. Additional synteny was revealed by the presence of similar *TatD* homologs located 128 and 215 bp upstream from the *SyA-Cph1* and *SyB-Cph1* coding regions, respectively, which are predicted to be separate transcriptional units (Fig. 1*A*). At this time, functional connectivities between the DUF309 and TatD-related proteins and the Cphs are not obvious. *E. coli* TatD has been classified as a magnesium-dependent cytoplasmic deoxyribonuclease (55).

SyA-Cph1 and SyB-Cph1 Assemble with PCB to Generate Photochromic Phys—Given their potential thermostability and the possibility that the 200-amino acid GAF alone can complete Pr → Pfr photoconversion, we predicted that *SyA*-Cph1 and *SyB*-Cph1 might be advantageous for various physicochemical analyses of Phy-type receptors. Full-length polypeptides of both bearing a C-terminal His_6 tag expressed well in *E. coli* but were completely insoluble. Fortunately, truncated variants of each encompassing just the GAF domain or the GAF domain in combination with the PHY domain expressed well, were highly soluble, and could be easily purified by nickel-chelate affinity chromatography followed by hydrophobic FPLC.

To test for their ability to assemble with bilins, we incubated purified *SyA*-Cph1(GAF) and *SyB*-Cph1(GAF) apoproteins with PCB or BV *in vitro* and then assayed for covalent attachment by zinc-induced fluorescence of the products following SDS-PAGE (8). As can be seen in Fig. 2, these GAF-only constructions, like a PAS-GAF-PHY fragment from *Syn*-Cph1 (11, 12), readily bound PCB but not BV. In contrast, a PAS-GAF-PHY fragment from the *Dr*BphP more effectively bound BV under identical conditions, consistent with its preference for BV (8, 56). Sequence alignments with other members of the Phy superfamily identified Cys-138 as the likely bilin attachment site for *SyB*-Cph1 (Fig. 1*B*). In support, a Cys-138 to alanine substitution in *SyB*-Cph1(GAF) effectively abrogated PCB ligation (Fig. 2).

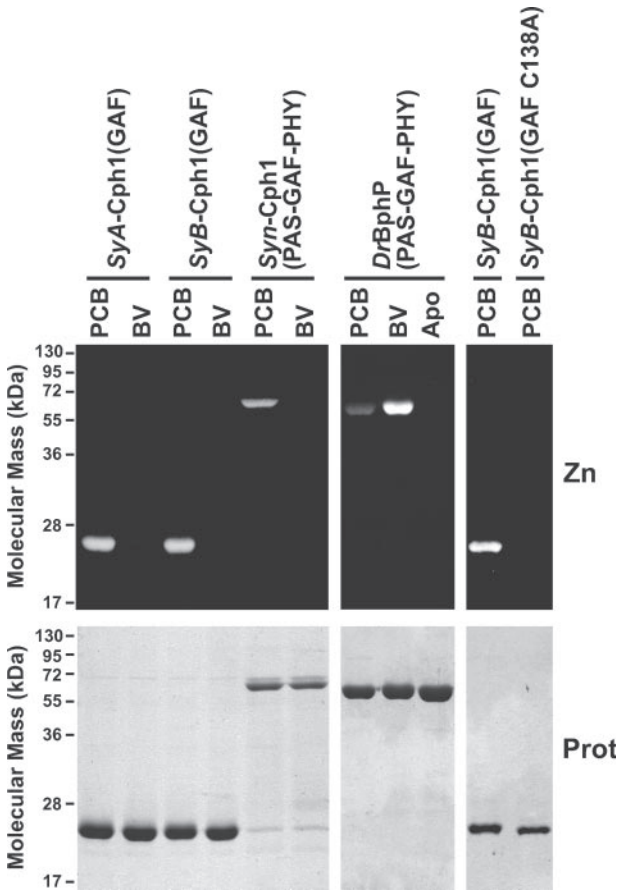

FIGURE 2. ***In vitro* assembly of *SyA*-Cph1 and *SyB*-Cph1 with PCB.** Recombinant GAF polypeptides from *SyA*-Cph1, *SyB*-Cph1, and *SyB*-Cph1(GAF) polypeptide where Cys-138 was substituted for an alanine, and PAS-GAF-PHY polypeptides from *D. radiodurans* (*Dr*BphP) and *Synechocystis* (*Syn*) were incubated with PCB or BV and purified by nickel-chelate affinity chromatography. Samples were subjected to SDS-PAGE and either assayed for the bound bilin by zinc-induced fluorescence (*Zn*), or stained for protein with Coomassie Blue (*Prot*). *Apo,* apoprotein before incubation with the bilin.

To scale-up *SyA*-Cph1 and *SyB*-Cph1 chromoprotein production, we exploited the dual-plasmid *E. coli* system of Gambetta and Lagarias (38), which co-expresses the apoprotein with the HO and BVR enzymes needed to synthesize PCB from heme. Absorption spectra of the resulting *in vivo* assembled photoreceptors, either spanning the GAF-PHY region or just the GAF domain, resembled typical Phys and were photochromic following red and far-red light irradiations (Fig. 3). The Pr absorption spectra of the GAF-PHY fragments have maxima at 630 nm for the Q bands, which are blue-shifted relative to the Pr form generated by the PAS-GAF-PHY or PAS-GAF fragments

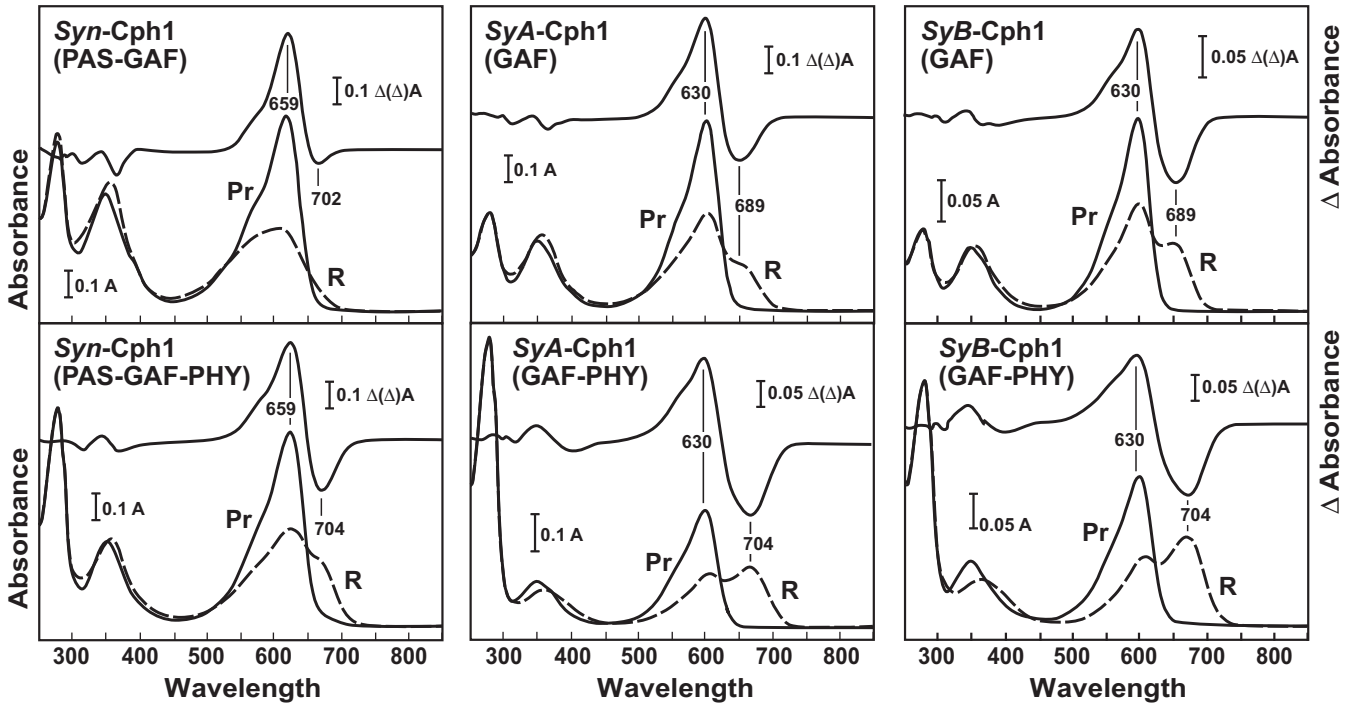

FIGURE 3. **UV-visible absorption spectra of PCB-assembled *SyA*-Cph1 and *SyB*-Cph1 encompassing only the GAF domain or the GAF-PHY region as Pr (*solid lines*) or following saturating red light (*R*) irradiation (mostly Pfr, *dashed lines*).** Pr-minus-Pfr difference spectra with their maxima and minima are shown *above*. The absorption and difference spectra of PAS-GAF and PAS-GAF-PHY regions of *Syn*-Cph1 assembled with PCB are included for comparison.

from *Syn*-Cph1 with absorption maxima at 659 nm (Fig. 3) (12, 14). Saturating red light irradiations of the GAF-PHY fragments from *SyA*-Cph1 and *SyB*-Cph1 converted most Pr to Pfr with absorption maxima at 704 nm, much like *Syn*-Cph1(PAS-GAF-PHY) (Fig. 3).

In contrast to truncations of other Phys that are missing the PHY domain, including *Syn*-Cph1 and *Dr*BphP that are poorly photochromic (Fig. 3) (15, 19), the *SyA*-Cph1(GAF) and *SyB*-Cph1(GAF) constructions retain most of their red/far-red light photoreversibility. Saturating red light transformed a substantial portion of the PCB-bound GAF polypeptides to a species resembling Pfr. This photoconversion was more efficient for *SyB*-Cph1(GAF), which produced a defined Pfr absorption peak at 689 nm in saturating red light (Fig. 3).

SEC has shown that most, if not all, intact Phys are dimeric with their binding interface(s) involving one or more regions, including the GAF domain in *Dr*BphP (13), the PAS-GAF-PHY domain in *Syn*-Cph1 (30, 57), and the C-terminal HK and HK-related regions in microbial and higher plants Phys (58–60). Similar SEC analysis of the GAF and GAF-PHY constructions of *SyB*-Cph1 assembled with PCB indicated that the PHY domain helps this chromoprotein dimerize. Whereas the GAF domain alone as Pr behaved as a monomer of 22 kDa, consistent with its calculated molecular mass of 23.3 kDa, the GAF-PHY fragment eluted as a dimeric species at 105 kDa, nearly twice the size of its calculated mass of 48.4 kDa (supplemental Fig. 3). The SEC elution profiles of both GAF and GAF-PHY constructions of *SyB*-Cph1 were indistinguishable following exposure to saturating red light, suggesting that their overall shapes and dimerization status are not dramatically altered upon photoconversion (supplemental Fig. 3).

SyA-Cph1 and SyB-Cph1 Are Thermostable—Synechococcus sp. OS-A and OS-B′ grow well between 54 and 63 °C with an optimum growth temperature of 60 °C (45). By exposing recombinant *SyA*-Cph1 and *SyB*-Cph1 chromoproteins to a wide range of temperatures, we confirmed that the photoreceptors are likewise thermotolerant. The GAF constructions of *SyA*-Cph1 and *SyB*-Cph1 had denaturation temperatures (temperature where 50% of the protein becomes insoluble) of 76 and 83 °C, respectively, which decreased slightly to 72 and 76 °C, respectively, upon inclusion of the PHY domain (Fig. 4*A*). By contrast, the PAS-GAF and PAS-GAF-PHY chromoproteins from *Syn*-Cph1, which were derived from the mesophilic *Synechocystis* sp. PCC6803 species, denatured at 54 and 53 °C, respectively (Fig. 4*A*).

Thermostable enzymes typically work more efficiently at higher temperatures, with optimal performance often matching the preferred growth temperature of the host organism (61). This expectation may also hold true for the Pr/Pfr interconversion of *SyA*-Cph1 and *SyB*-Cph1. Both the GAF and GAF-PHY constructions of *SyB*-Cph1 were more efficient at Pr → Pfr photoconversion at 65 °C *versus* 23 °C using the same fluence rate of red light (initial rates increased by ~3- and 2-fold, respectively) (Fig. 4*B* and supplemental Fig. 4*A*). Because the primary photochemical event should be relatively temperature-insensitive, much of this increased rate likely reflects accelerated thermal relaxation steps from the Lumi-R intermediate to Pfr. Subsequent Pfr → Pr thermal reversion of the GAF chromoprotein was also faster at 65 *versus* 23 °C, with the initial rate increased by 9-fold at the higher temperature (Fig. 4*C*). Surprisingly, little thermal reversion occurred at 23 °C for the GAF-PHY construction of *SyB*-Cph1 even after 12 h of dark incuba-

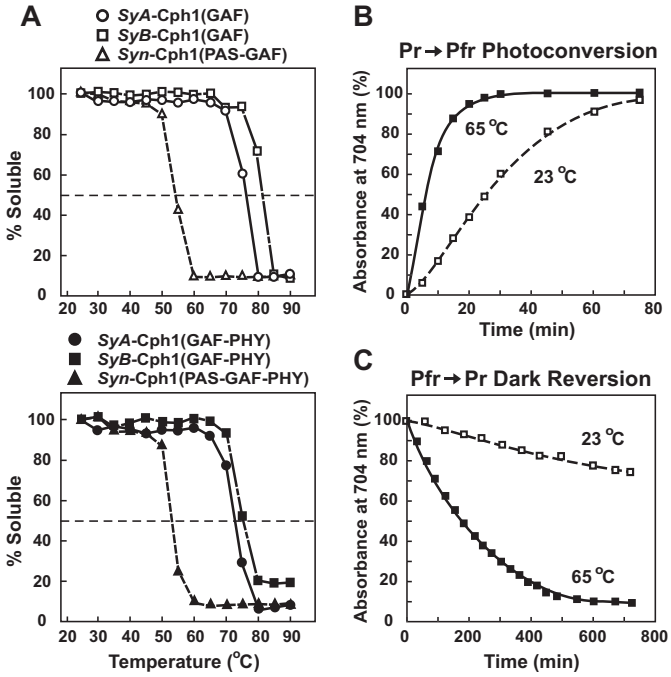

FIGURE 4. **Thermostability of the *SyA*-Cph1 and *SyB*-Cph1 chromoprotein.** Recombinant GAF and GAF-PHY fragments of *SyA*-Cph1 and *SyB*-Cph1 were assembled with PCB *in vivo* and purified by nickel-chelate affinity chromatography. *A*, solubility of the chromoproteins upon exposure to increasing temperatures. PAS-GAF and PAS-GAF-PHY fragments of *Syn*-Cph1 from the mesophilic *Synechocystis* sp. PCC6803 species are included for comparison. *B* and *C*, effect of temperature (23 *versus* 65 °C) on Pr → Pfr photoconversion by red light (*B*) and Pfr→Pr dark reversion (*C*) of *SyB*-Cph1(GAF) assembled with PCB.

tion (supplemental Fig. 4*B*), suggesting that even lower temperatures might effectively stabilize the Pfr form of this fragment.

SyB-Cph1 Mutant Affecting Asp-86 Emits Intense Red Fluorescence—Random and structurally guided mutagenesis of Phys have identified a number of conserved residues important for photochemistry. As examples, replacement of Tyr-176 in *Syn*-Cph1 with a histidine generates a highly red fluorescent chromoprotein that cannot photoconvert to Pfr (17, 52), whereas various substitutions of Asp-207 (*e.g.* D207H variant) block Pr → Pfr photoconversion in *Dr*BphP (19). To further compare the binding pocket of these PAS-less Phys relative to more typical Phys, analogous mutations (Y54H and D86H (Fig. 1*B*)) were introduced into the GAF and GAF-PHY constructions of *SyB*-Cph1.

Both sets of Y54H and D86H variants in *SyB*-Cph1 were soluble, retained their ability to bind PCB (Fig. 5*A*), and generated near normal absorption spectra for the Pr state with Q band maxima at or near 630 nm (Fig. 5*B*), in agreement with prior studies with other Phys showing that these residues do not significantly affect Pr assembly (17–19). However, absorption spectra recorded after red light irradiation revealed substantial photochemical defects in the variants (Fig. 5*B*). For the *SyB*-Cph1(GAF) chromoprotein, both substitutions generated partially bleached photoproducts as judged by the loss of absorbance for the Pr form at 630 nm that was not accompanied by a commensurate absorbance increase for Pfr at 689 nm. Upon inclusion of the PHY domain, a similar mild effect was evident for the Y54H substitution. However, the *SyB*-Cph1(GAF-PHY D86H) substitution was strongly blocked in its ability to photoconvert. The absorption spectrum of this variant was only slightly affected by saturating red light. The small loss of absorbance at 630 nm that was observed was not associated with a concomitant increase in absorbance in the far-red wavelength region for Pfr, indicating that most Pr → Pfr photoconversion was inhibited.

Similar photochromic defects were evident in comparable substitutions of *Syn*-Cph1 (both PAS-GAF and PAS-GAF-PHY truncations), but the effects were stronger with the tyrosine variants (Fig. 5). In agreement with Fischer *et al.* (17, 52), the Y176H variant introduced into both *Syn*-Cph1 constructions strongly compromised Pr → Pfr photoconversion with saturating red light generating little or no Pfr. By contrast, the absorption spectrum of the *Syn*-Cph1(PAS-GAF D207H) variant after treatment with saturating red light produced a "bleached" photoproduct similar to its wild-type counterpart. The *Syn*-Cph1(PAS-GAF-PHY D207H) mutant also retained its ability to photoconvert in red light, but instead of generating the far-red light-absorbing Pfr-like state, it transformed to an unexpected blue-shifted species with a well defined absorption maximum at 592 nm. The mechanism responsible for this unorthodox hypsochromic shift is not known, but it could resemble the Pnr state of the novel Phy (*Rp*BphP3) recently described from *R. palustris* (7, 53). *Rp*BphP3 does not photoconvert from Pr to Pfr in red light but instead generates this blue-shifted Pnr species.

When the fluorescent properties of the set of *SyB*-Cph1 and *Syn*-Cph1 variants were analyzed, similar differential defects were observed that roughly paralleled the effects of the variants on Pr → Pfr photoconversion (Fig. 6). In accord with previous studies (17, 52), introduction of the Y176H mutation into either the PAS-GAF or PAS-GAF-PHY constructions of *Syn*-Cph1 generated red fluorescent chromoproteins with strong emission maxima at 662 nm. The PAS-GAF-PHY Y176H variant was approximately three times more fluorescent than the equivalent PAS-GAF construction. Neither the wild-type chromoproteins nor constructions bearing the D207H mutation were fluorescent.

The opposite trend occurred for *SyB*-Cph1 in addition to a much greater overall fluorescence yield (Fig. 6). Like the wild-type GAF and GAF-PHY constructions of *SyB*-Cph1, the corresponding Y54H substitutions were moderately fluorescent, with emission maxima at 646–654 nm. In contrast, the D86H substitutions were substantially more fluorescent with the *SyB*-Cph1(GAF-PHY D86H) variant showing especially strong fluorescence output. Excitation maxima were evident at 357, 379, 591, and 620 nm with a single emission peak at 650 nm. By comparing fluorescence emission using equivalent amounts of chromoprotein (based on equal absorbance of the Pr Q band), the *SyB*-Cph1(GAF-PHY D86H) chromoprotein was ~3.5 times more fluorescent than the comparable chromoprotein without the PHY domain and was five times more fluorescent when compared with the *Syn*-Cph1(PAS-GAF-PHY Y176H) chromoprotein.

Resonance Raman (RR) Spectroscopy of SyB-Cph1—The sequence homology within the GAF domains of *SyA*-Cph1 and

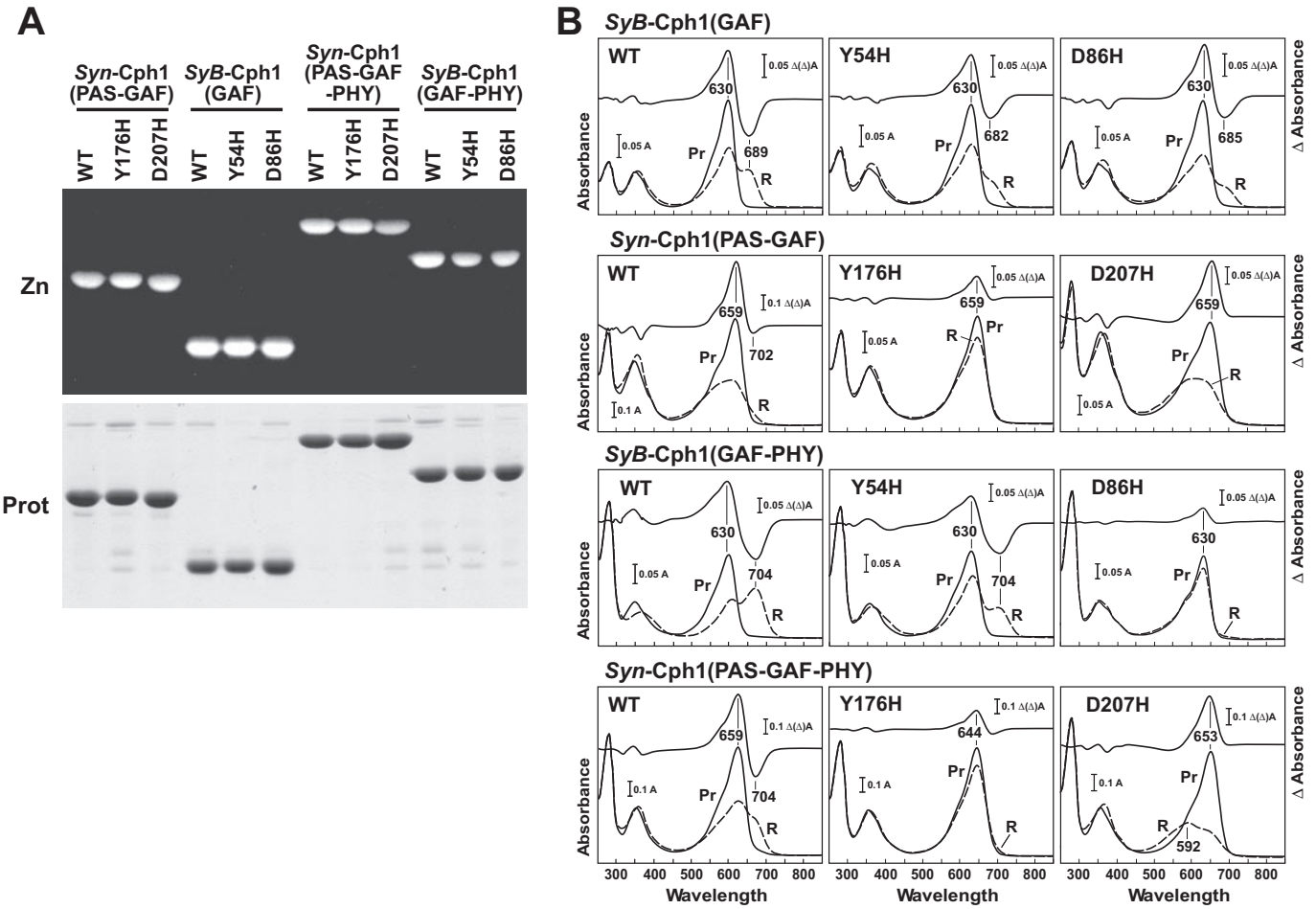

FIGURE 5. **Effects of positionally conserved tyrosine and aspartic acid residues on assembly of *SyB*-Cph1 and *Syn*-Cph1 with PCB and the absorption spectra of the resulting chromoproteins.** GAF and GAF-PHY polypeptides from *SyB*-Cph1 and PAS-GAF and PAS-GAF-PHY polypeptides from *Syn*-Cph1 bearing histidine substitutions for the tyrosine (residue 54 and 176 in *SyB*-Cph1 and *Syn*-Cph1, respectively) or aspartic acid (residue 86 and 207 in *SyB*-Cph1 and *Syn*-Cph1, respectively) were co-expressed with PCB and purified by nickel-chelate affinity chromatography. *A*, ability of the mutant apoproteins to bind PCB. Samples were subjected to SDS-PAGE and either assayed for the bound bilin by zinc-induced fluorescence (*Zn*) or stained for protein with Coomassie Blue (*Prot*). *B*, UV-visible absorption spectra of the mutants shown in *A* as Pr (*solid lines*) or following saturating red light (*R*) irradiation (mostly Pfr, *dashed lines*). Pr-minus-Pfr difference spectra with their difference maxima and minima are shown above. *WT*, wild type.

SyB-Cph1 relative to more typical Phys strongly suggested that these PAS-less Phys adopt a similar bilin geometry and employ a similar reaction mechanism to generate Pfr from Pr, including the use of a deprotonation/reprotonation cycle during the relaxation steps from Lumi-R to Pfr (2, 18, 19). To help confirm this expectation, we employed RR spectroscopy to assess bilin conformation and protonation state. In particular, RR bands in the region between 1500 and 1700 cm^{-1} can (i) help predict the methine bridge configurations and conformations (*i.e. Z/E* and *syn*/*anti* geometries), (ii) reveal the protonation state of the pyrrole nitrogens in the Pr and Pfr states, and (iii) detect the accumulation of transformation intermediates if complete photoconversion stalls (*e.g.* deprotonated Meta-R_c intermediate (18, 24, 43, 62, 63)). Moreover, by comparing the RR spectra of the GAF and GAF-PHY constructions, we could define the importance of the PHY domain during Pr → Pfr photoconversion for these thermostable PAS-less Phys.

The RR spectra of the Pr state of *SyB*-Cph1(GAF) and *SyB*-Cph1(GAF-PHY) displayed very similar overall vibrational band patterns (supplemental Fig. 5). These data agreed with previous studies demonstrating that the PHY domain has little impact on Pr absorption (15, 19, 26) and bilin geometry (10, 19). In particular, RR bands attributed to the methine bridge geometry of PCB (1600–1650 cm^{-1}) (63) and subtle details of the bilin structure (600–900 cm^{-1}) were identical or very similar for *SyB*-Cph1(GAF) and *SyB*-Cph1(GAF-PHY) (Fig. 7 and supplemental Fig. 5). The N-H in-plane bending mode of pyrrole rings B and C in Pr, assigned based on its disappearance in D_2O (43), was at similar positions for both chromoproteins (1573 *versus* 1575 cm^{-1} (Fig. 7)). These data imply that PCB retained its protonation (cationic) state and that its hydrogen bond interactions with the protein environment were for the most part unaffected by removal of the PHY domain. Only subtle differences were evident in the region between 1400 and 1500 cm^{-1}, which could reflect slightly greater contributions from protein Raman bands in the *SyB*-Cph1(GAF-PHY) (supplemental Fig. 5).

The RR spectra of the Pr state of *SyB*-Cph1(GAF) and *SyB*-Cph1(GAF-PHY) differed from that obtained with *Syn*-Cph1(PAS-GAF-PHY), suggesting that subtle differences in bilin geometry exist between the two Cph classes. The marker band region for protonated bilins (1600–1650 cm^{-1}) is usually

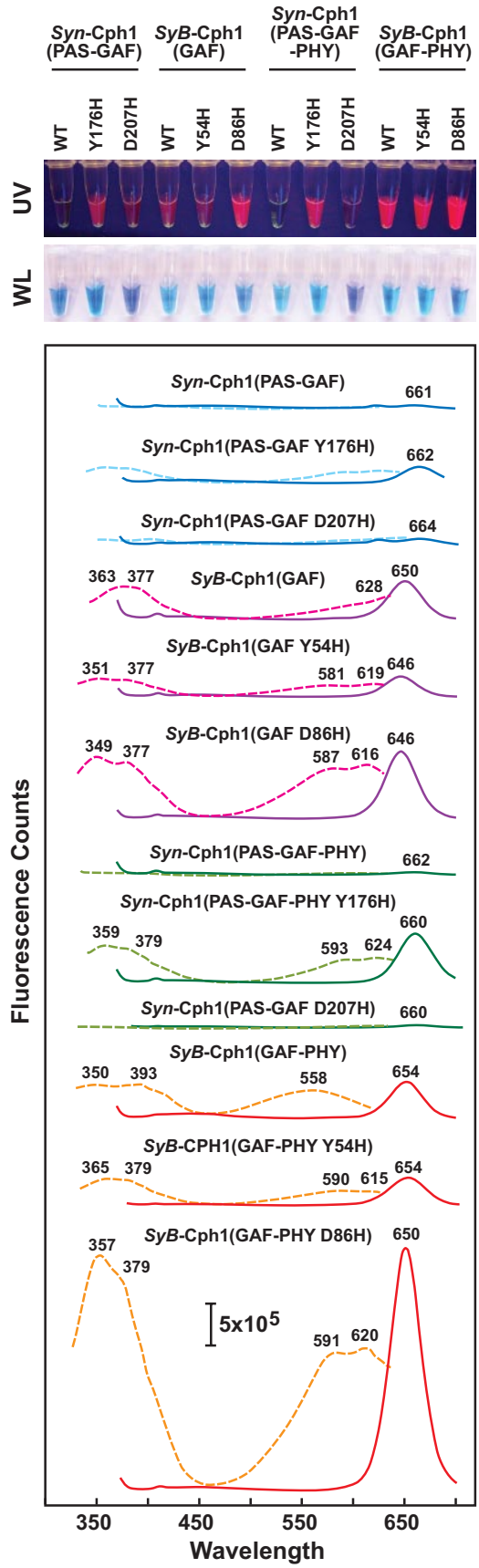

FIGURE 6. **Fluorescence characteristics of the tyrosine and aspartic acid substitutions in *Syn*-Cph1 and *SyB*-Cph1.** PCB binding and absorption spectra of the mutants are shown in Fig. 5. All samples were adjusted to have a 0.6 absorbance at the Pr absorption maximum. *Top panels,* purified chromoprotein solutions upon irradiation with UV light (*UV*) or white light (*WL*). *Bottom spectra,* fluorescence excitation (*dashed lines*) and emission spectra (*solid lines*) of the chromoprotein samples shown at *top*. Excitation and emission maxima are indicated.

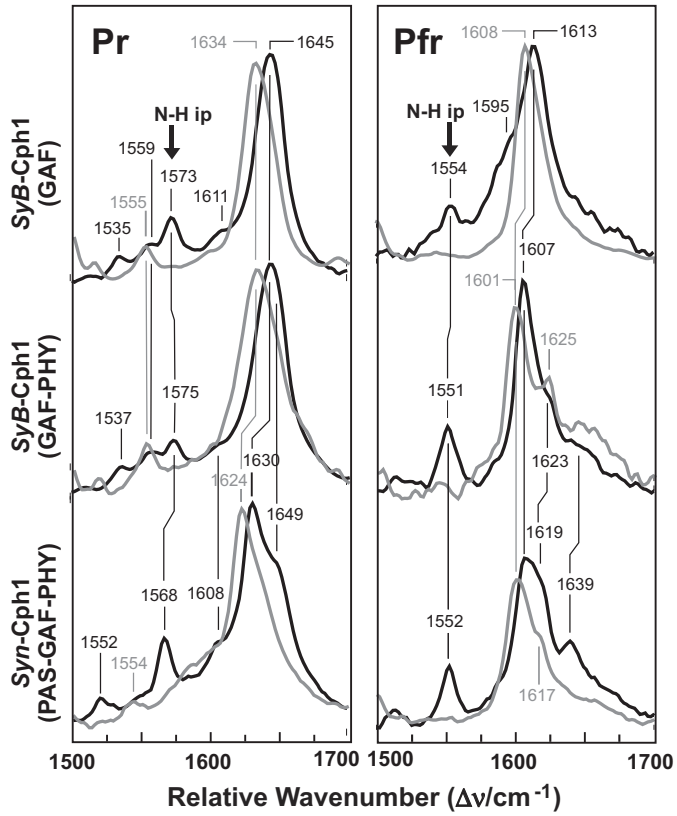

FIGURE 7. **RR spectra of the Pr and Pfr forms of the GAF and GAF-PHY fragments of *SyB*-Cph1 as compared with the PAS-GAF-PHY fragment from *Synechocystis*.** RR spectra were recorded between 1500 and 1700 cm^{-1} for Pr (*left panel*) and after saturating red light (mostly Pfr, *right panel*). Samples were measured in the presence of H_2O (*black lines*) or D_2O (*gray lines*). The positions of the pyrrole N-H in-plane bending (*ip*) modes are marked by the *arrows*. RR spectra for *Syn*-Cph1(PAS-GAF-PHY) were taken from Ref. 75.

dominated by two species originating from the C=C stretching modes of the ring-A-B and -C-D methine bridges (63); these can be seen as a prominent band (1630 cm^{-1}) and a shoulder (1649 cm^{-1}) in the RR spectrum of *Syn*-Cph1(PAS-GAF-PHY) (Fig. 7). However, for *SyB*-Cph1(GAF) and *SyB*-Cph1(GAF-PHY), the 1630-cm^{-1} band seemed to be upshifted to nearly coincide with the higher frequency mode, thus creating a single symmetric band at 1645 cm^{-1} (Fig. 7). This shift most likely reflects a conformational difference at the C-D bridge as compared with *Syn*-Cph1(PAS-GAF-PHY). This structural difference may also affect hydrogen bonding of the ring-C N-H group as indicated by the 7-cm^{-1} higher in-plane bending frequency of the N-H group for *SyB*-Cph1(GAF-PHY) (1575 cm^{-1}) compared with *Syn*-Cph1(PAS-GAF-PHY) (1568 cm^{-1}). In contrast, RR spectra provide no indication for structural differences at the A-B and B-C methine bridges because the corresponding stretching bands at 1649 cm^{-1} (A-B) and 1609 cm^{-1} (B-C) were largely unchanged in *SyB*-Cph1(GAF-PHY) *versus* *Syn*-Cph1(PAS-GAF-PHY) (Fig. 7).

Differences in absorption spectra of *SyB*-Cph1(GAF) and *SyB*-Cph1(GAF-PHY) following red light suggested that the GAF domain by itself is not fully competent in forming Pfr (Fig. 3). However, in contrast to other prokaryotic Phys that lack the PHY domain (19, 43, 62), RR spectra revealed the *SyB*-Cph1(GAF) fragment does not arrest in a Meta R_c-like intermediate upon red light irradiation. Instead, several signature RR bands of the *SyB*-Cph1(GAF) photoproduct were consistent with the accumulation of Pfr. Included were a drastic downshift of the C-D methine bridge stretching from 1645 cm^{-1} in Pr to 1613 cm^{-1} and ring-B and -C N-H in-plane bending mode at 1554 cm^{-1}, which is characteristic of the protonated Pfr state (43, 62) (Fig. 7). Only the shoulder at ~1595 cm^{-1} in the RR spectrum of the Pfr-like state of *SyB*-Cph1(GAF) is reminiscent of a Meta-R_c-like species (24) (Fig. 7). However, this band was not observed in D_2O leaving its assignment ambiguous.

The most significant difference in the RR spectra of the photoconversion products between the GAF and GAF-PHY constructions of *SyB*-Cph1 was a large intensity reduction in the band at ~813 cm^{-1} (supplemental Fig. 5). This band originates from the C-H out-of-plane mode of the C-D methine bridge (43, 64); its high RR intensity, which is a typical feature of the Pfr chromophore, may reflect torsion of the C-D methine bridge. Furthermore, the A-B stretching could not be identified as a distinct peak or shoulder in *SyB*-Cph1(GAF) as it may overlap with the dominant 1613-cm^{-1} band. Instead, the RR spectra of the Pfr states for *SyB*-Cph1(GAF-PHY) and *Syn*-Cph1(PAS-GAF-PHY) display two bands at ~1620 and 1640 cm^{-1}, which both are possible candidates for the A-B stretching, thus pointing to a conformational heterogeneity at the A-B methine bridge. These differences suggest that the PHY domain subtly affects the chromophore-protein architecture of *SyB*-Cph1 in the Pfr state with respect to the structural details of the A-B and C-D methine bridges.

One-dimensional and Two-dimensional NMR Analysis of PCB Bound to SyB-Cph1(GAF)—The fact that the 200-amino acid GAF domain of *SyB*-Cph1 retains its bilin lyase activity and most of its red/far-red photochromicity and behaves as a monomer indicated that this fragment could help visualize by NMR spectroscopy global movements of a Phy chromophore and its binding pocket during phototransformation. Toward this goal, we synthesized and assembled *SyB*-Cph1(GAF) holoproteins in which either PCB or the polypeptide were labeled individually with ^{15}N and/or ^{13}C. Incorporation of isotopically labeled PCB into unlabeled protein was accomplished by replacing the bilin precursor ALA, added in excess to the growth medium, with either ^{15}N- or ^{13}C-labeled derivatives. Incorporation of ^{15}N and ^{13}C into the polypeptide was achieved by replacing NH_4Cl and glycerol in the medium with ^{15}N- and ^{13}C-labeled counterparts, respectively, together with an excess of unlabeled ALA. For a visual aid, Fig. 8*A* shows the predicted position of the ^{13}C-labeled carbons incorporated into PCB upon addition of 1,2-[^{13}C]ALA to the medium.

Prior one-dimensional ^{15}N NMR analysis of *Syn*-Cph1(PAS-GAF-PHY) assembled with [^{13}C-^{15}N]PCB *in vitro* detected all four pyrrole ring nitrogens in the Pr conformer, with three new distinct peaks appearing after red light irradiation (32, 33). These spectra implied that at least three of the chromophore

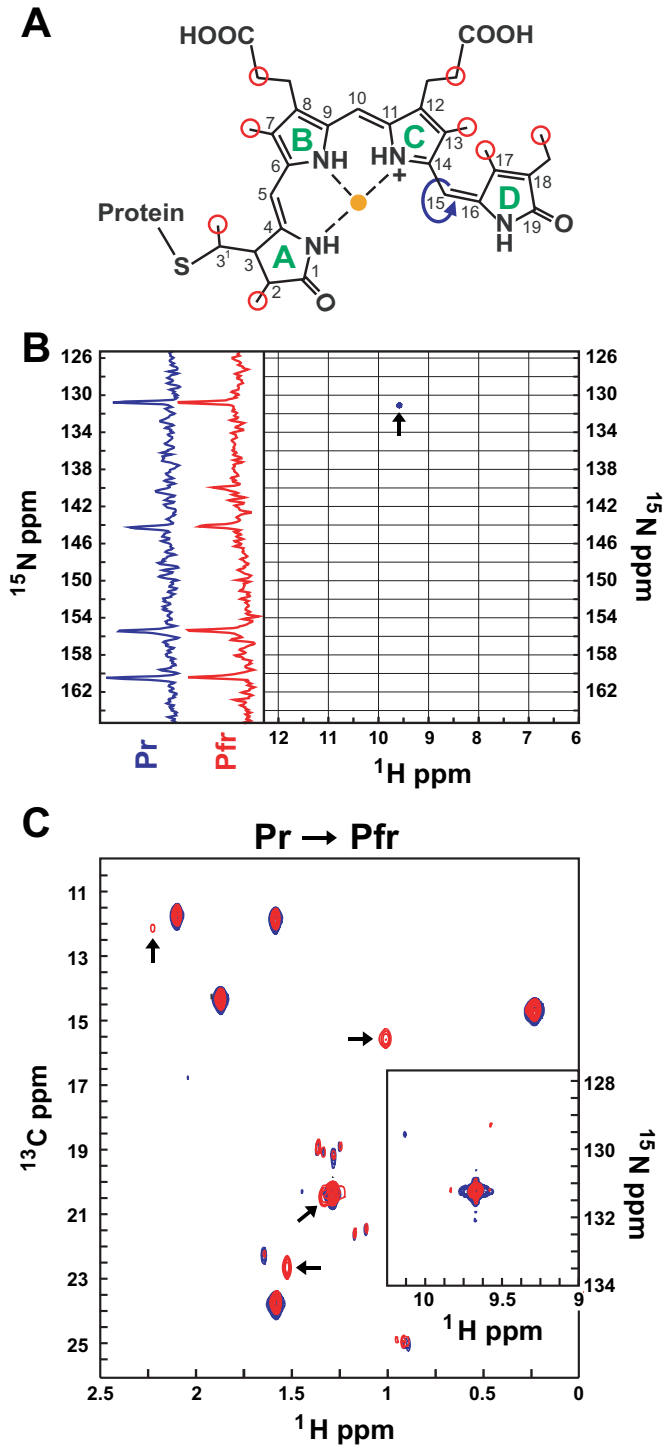

FIGURE 8. **One-dimensional ^{15}N spectra and two-dimensional ^{1}H-^{15}N and ^{1}H-^{13}C HSQC NMR spectra of *SyB*-Cph1(GAF) assembled with isotopically labeled [^{15}N]PCB or [^{13}C] PCB.** *A*, location of the PCB carbons (*circled* in *red*) labeled with ^{13}C using the heme precursor 1,2-[^{13}C]ALA. PCB is diagrammed in the predicted *ZZZ-syn,syn,anti* conformation for Pr (34). The *blue arrow* shows the predicted *Z* to *E* rotation around the C-15–C-16 double bond during photoconversion from Pr to Pfr. The position of the pyrrole water that is coordinated by the A-, B-, and C-pyrrole ring nitrogens is shown in *orange*. *B*, one-dimensional ^{15}N NMR spectra of [^{15}N]PCB *SyB*-Cph1(GAF) as Pr (*blue*) or following saturating red light (mostly Pfr, *red*), and a two-dimensional ^{1}H-^{15}N HSQC spectrum of the same sample in Pr. *C*, ^{1}H-^{13}C and ^{1}H-^{15}N HSQC spectra of *SyB*-Cph1(GAF) containing isotopically labeled PCB either as Pr (*blue*) or following saturating red light (mostly Pfr, *red*). PCB was either uniformly labeled with ^{15}N (*inset*) or assembled with [^{13}C]PCB isotopically labeled at the positions shown in *A*. *Arrows* identify new peaks that appeared during red light irradiation.

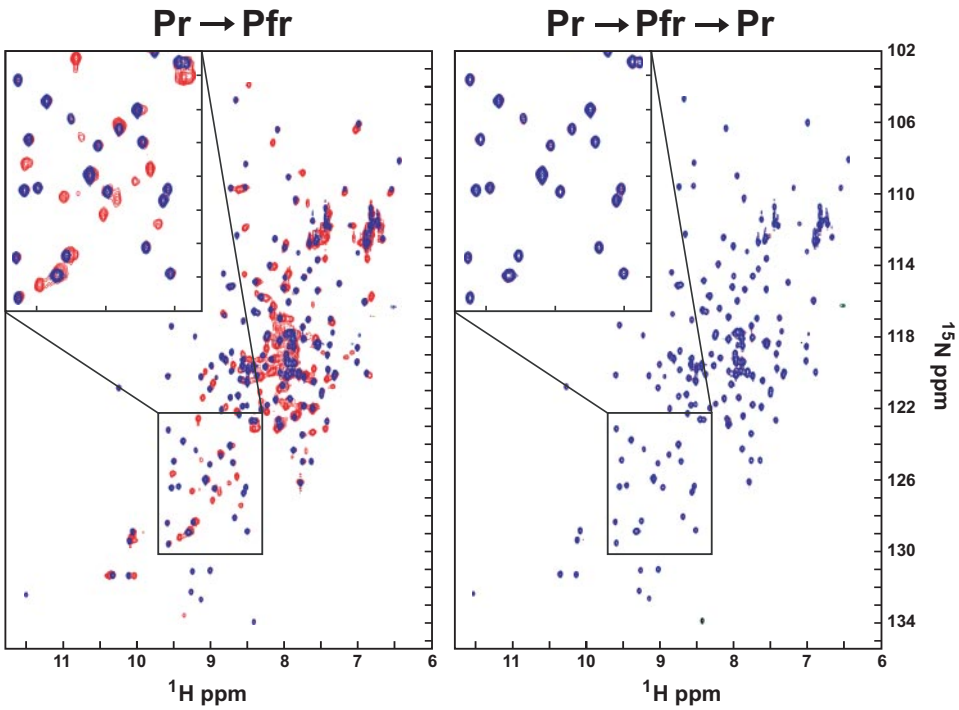

FIGURE 9. **Two-dimensional ^{1}H-^{15}N HSQC NMR spectra of [^{15}C-^{15}N]-*SyB*-Cph1(GAF) assembled with PCB.** NMR data were collected with four scans over a 20-min period with 2 mM [^{15}N-^{13}C]-*SyB*-Cph1(GAF) dissolved in 7% D_2O 10 mM Tris-DCl (pH 8.5). *Left panel,* two-dimensional NMR spectrum of Pr (*blue*) overlaid on that obtained during continuous *red light* irradiation (mostly Pfr, *red*). *Right panel,* two-dimensional NMR spectrum of Pr (*blue*) overlaid on that obtained for a sample exposed to saturating red light (mostly Pfr) followed by saturating far-red light (regenerated Pr, *red*). The *insets* are magnifications of regions in the ^{1}H-^{15}N HSQC spectra which included a number of peaks that substantially change position upon Pfr formation.

nitrogens significantly change their geometry/chemical environment during Pr → Pfr photoconversion. A similar one-dimensional NMR spectrum was obtained here for the Pr conformer of *SyB*-Cph1(GAF) assembled with uniformly labeled [^{15}N]PCB (Fig. 8*B*). Four distinct peaks were evident in the ^{15}N spectrum representing each of the four pyrrole nitrogens. That these peaks were below 180 ppm was consistent with all of these nitrogens being protonated at neutral pH (65, 66). Interestingly, for *Syn*-Cph1(PAS-GAF-PHY) two of these peaks overlapped, indicative of similar chemical environments (32, 33), whereas in *SyB*-Cph1(GAF) they were more uniformly resolved, indicative of more distinct chemical environments (Fig. 8*B*).

The positions of three of the four one-dimensional ^{15}N NMR peaks (131, 155, and 160 ppm) from *SyB*-Cph1(GAF) were unaffected by red light irradiation, implying that the environments of these pyrrole nitrogens do not detectably change upon photoconversion to Pfr (Fig. 8*B*). A decrease in signal was observed for the fourth ^{15}N peak at 144 ppm coincident with the appearance of a new ^{15}N peak at 142 ppm, suggesting that this pyrrole nitrogen experiences a new environment upon Pr → Pfr photoconversion. Surprisingly, two-dimensional ^{1}H-^{15}N HSQC of [^{15}N]PCB-labeled *SyB*-Cph1(GAF) as Pr revealed only a single H-N correlation peak at 131 ppm (Fig. 8*B*), which did not change position or intensity upon red light exposure (Fig. 8*C*, *inset*). This failure to detect additional H-N correlation peaks implied that that the protons associated with three of the four pyrrole nitrogens readily exchange with the solvent.

To examine movements of the PCB carbons in *SyB*-Cph1(GAF), we used 1,2-[^{13}C]ALA as the PCB precursor to label all six methyl groups and C8^{2} and C12^{2} methylene carbons present in the B- and C-ring propionate side chains, respectively (67) (Fig. 8*A*). Two-dimensional NMR ^{1}H-^{13}C HSQC spectra with the sample as Pr detected peaks for the expected six methyl groups (Fig. 8*C*). However, we did not observe peaks for the two propionate methylene carbons, suggesting that they are highly mobile in the Pr conformation. The positions of the ^{1}H-^{13}C peaks for the methyl groups as Pr were similar to those described by Strauss *et al.* (32) for *Syn*-Cph1(PAS-GAF-PHY). Taken together with similar RR spectra (supplemental Fig. 5), it appears that the Pr conformer of *SyB*-Cph1 has a bilin geometry similar to that for *Syn*-Cph1 even without the PAS domain. Upon saturating red light irradiation, several new peaks appeared in the ^{1}H-^{13}C HSQC spectra of [^{13}C]PCB *SyB*-Cph1(GAF) that can be readily seen by overlaying this spectrum with that for Pr (Fig. 8*C*). These new peaks likely reflect movement of several PCB methyl groups to new chemical environments during Pr → Pfr photoconversion.

Two-dimensional NMR Analysis of ^{15}N-^{13}C-Labeled SyB-Cph1(GAF) Reveals Global Movement in the GAF Domain during Photoconversion—To study global movements of the GAF domain polypeptide during Pr → Pfr photoconversion, we synthesized ^{15}N and ^{13}C double-labeled *SyB*-Cph1(GAF) chromoprotein. Presumably because of its stability and small size (208 amino acids), this sample generated highly resolved two-dimensional ^{1}H-^{15}N HSQC spectra as Pr (Fig. 9*A*). The number of detected ^{1}H-^{15}N peaks was reasonably close to the expected number generated from the predicted 208-amino acid His_6-tagged *SyB*-Cph1(GAF) chromoprotein with the addition of some observable side-chain resonances.

When the ^{15}N-^{13}C-labeled *SyB*-Cph1(GAF) sample was photoconverted to Pfr by saturating red light and then maintained in this photoequilibrium during data collection by continuous red light irradiation, a remarkably distinct ^{1}H-^{15}N HSQC spectrum was captured. When overlaid with the original Pr plot, the two-dimensional NMR Pr/Pfr spectrum not only contained the same ^{1}H-^{15}N peaks observed with Pr (Fig. 9*A*, *peaks colored* in *blue*), thus reflecting residual Pr at photoequilibrium, it also contained numerous new ^{1}H-^{15}N peaks that reflected the movement of various amide groups specific to Pfr (Fig. 9*A*, *peaks colored* in *red*). Close inspection identified chemical shift changes (reflecting chemical and magnetic environmental changes) for ~50% of the residues within the GAF domain

upon photoconversion. Based on preliminary residue assignments, many of these changes are small to moderate, but a few large (2–3 ppm ^{13}C or ^{15}N) backbone chemical shift changes could be observed (data not shown). Moreover, when red light-irradiated samples were converted back to Pr, either by extended darkness or by subsequent irradiation with saturating far-red light, all Pfr-associated peaks returned back to their original Pr positions (Fig. 9*B* and data not shown). This photoreversibility demonstrated that the new peaks observed after red light irradiation were not generated by denaturation or photobleaching of the sample, but likely reflected the signature photochromicity of Phys. This measurement thus represents the first assessment of the global movements of a Phy CBD during Pr → Pfr photoconversion in solution and indicates that the conformation of the GAF domain in the Pr and Pfr conformers could differ substantially.

DISCUSSION

Novel Features of SyA-Cph1 and SyB-Cph1 Enable Structural Analysis of Phys by NMR—The structural resolution of both Pr and Pfr will be essential to fully understand how Phys function at the atomic level. Although the Pr structures of two CBDs have recently been determined using x-ray crystallography (10, 13, 53), those for Pfr have not yet been solved for a variety of technical reasons. Crystallization of the Pfr state has been challenged by substantial contamination of Pr even after saturating red light and the instability of Pfr once formed, which for most Phys will revert thermally back to Pr (Fig. 4*C*) (2). Generating Pfr by irradiating diffraction quality Pr crystals with red light has also failed thus far. The crystals have either failed to photoconvert or dissolved (53, 68, 69),[4] implying that the crystal lattice containing Pr cannot accommodate the structural rearrangements that occur during Pr → Pfr photoconversion. Exploiting naturally occurring Phys that prefer Pfr as the most stable state is an alternative for crystallizations, but it remains unclear if these bathy-Phys structurally resemble the canonical Phys in which Pr is the most stable state (5, 6).

Solving the solution structure of Pfr using NMR is an attractive alternative, given the ability of this approach to resolve chemical shifts generated solely from Pfr by "subtracting" the NMR spectrum generated with Pr from that obtained after saturating red light irradiation. NMR approaches work best if the size of the protein complex in solution is below 35 kDa (35, 36). Unfortunately, the Phy CBDs studied to date exceed this size range, needing at least the 35-kDa PAS-GAF fragment to generate the Meta-R_c state from Pr and at least the ~55-kDa PAS-GAF-PHY fragment for full photoconversion (15, 18, 19, 70). These sizes are further increased by dimerization (19, 57), thus putting most previously described Phys outside the acceptable size range required for conventional NMR spectroscopy techniques.

Here we described two thermostable Cphs, *SyA*-Cph1 and *SyB*-Cph1, that belong to a new sub-class of Phys with unique features that are particularly amenable to NMR studies. They were discovered by a metagenomic sequencing project aimed at classifying thermotolerant species (45, 46). Like canonical Phys, *SyA*-Cph1 and *SyB*-Cph1 contain an obvious GAF domain that binds the bilin, followed by a PHY domain often essential for complete Pr → Pfr photoconversion, and end with an HK domain similar to those found in many two-component signaling receptors. The GAF domains of both contain all of the strongly conserved amino acids shown to be important for bilin binding and photochemistry (13, 15–19). *SyA*-Cph1 and *SyB*-Cph1 both have a positionally conserved cysteine, which like others within the Cph family (11, 12) appears to serve as the bilin linkage site. As expected this pair binds PCB effectively to generate red/far-red light photochromic photoreceptors. Unfortunately, given the insolubility of the full-length recombinant polypeptides, we do not yet know how Pr → Pfr photoconversion affects the phosphotransferase activity conferred by the distal HK domain.

Conservation of the GAF domain is further supported by the analysis of site-directed mutants affecting Tyr-54 and Asp-86 in *SyB*-Cph1, which have been shown to hold key functional roles in other Phys (16–19, 52). Like similar mutations in *Syn*-Cph1 and *Dr*BphP, replacement of these residues does not affect Pr assembly but can substantially affect Pfr formation. The D86H chromoproteins in particular are substantially blocked in Pr → Pfr photoconversion and are highly red fluorescent. The effect of the Y54H and D86H mutations contrasts those for *Syn*-Cph1 in which the comparable Y176H is strongly fluorescent, whereas the D207H mutant is poorly fluorescent (Fig. 6) (17, 52).

One unique feature of *SyA*-Cph1 and *SyB*-Cph1 is that they belong to a previously unknown subfamily of Cphs present in at least several cyanobacteria (including mesophiles) that lack the N-terminal PAS domain. This subfamily is distinct from *Syn*-Cph2 and its relatives by having a strongly conserved RIT motif at the beginning of the GAF domain and ending in an HK domain. Although the function(s) of the PAS domain in Phy signaling are not yet clear, its presence in most Phys studied to date across a wide range of species, including bacteria, cyanobacteria, fungi, and plants, implied that it serves an essential function (15).

Three-dimensional structures of the CBD (10, 13, 53) revealed that the PAS domain is tethered to the adjacent GAF domain by a figure-of-eight knot, created by threading the residues N-terminal to the PAS domain through a lasso loop between β9 and α7 of the GAF domain (based on the *Dr*BphP CBD structure (10)). The resulting anti-parallel three-helix bundle also contacts the B-ring propionate acid side chain of the bilin, thus connecting the PAS domain indirectly to the chromophore. Strikingly, even though the PAS domain is absent in the PAS-less RIT and *Syn*-Cph2-type subfamilies, their GAF domains have retained the extra sequence that forms the lasso loop and several conserved residues within that are central to the knot core (*e.g.* Ile-113, Leu-127, and Arg-133 in *SyB*-Cph1 (10, 19)). Why the loop sequences have been retained is unclear. Without the upstream sequences, these loops should be more flexible and extend into the solvent. One possibility is that the GAF domains of PAS-less Cphs still use this loop sequence to interact with PAS-like domains synthesized separately.

[4] J. R. Wagner, K. T. Forest, and R. D. Vierstra, unpublished data.

Regardless of its function, it is clear from ours and others studies (14, 47) that the PAS domain is not essential for photochromicity. Like *Syn*-Cph2 (14, 47), *SyA*-Cph1 and *SyB*-Cph1 can bind PCB covalently *in vitro* and become red/far-red light photochromic with the only substantive difference being a blue shift of the Pr absorption maxima. Similarly, *SyA*-Cph1 and *SyB*-Cph1 also contain a second GAF domain downstream of the PHY domain. For *Syn*-Cph2, this GAF2 sequence can bind PCB when expressed alone, but the resulting chromoprotein is not red/far-red photochromic (14, 47). By inference, it is possible that *SyA*-Cph1 and *SyB*-Cph1 can incorporate two bilin groups simultaneously.

In contrast to several other Phys (15, 19, 62), *SyB*-Cph1 (and likely *SyA*-Cph1) also appears less dependent on the PHY domain for photoconversion to Pfr. Absorption, RR, and NMR spectroscopy indicate that most of the *SyB*-Cph1(GAF) truncation photoconverts to the protonated Pfr-type state upon red light irradiation with only slight modifications of its spectral properties (*e.g.* 15-nm blue shift of Pfr absorption maximum). Combined with its monomeric size, the *SyB*-Cph1(GAF) fragment is well within the acceptable size range for NMR analysis of Pfr.

Another important feature of these Phys is their remarkable heat stability, being capable of withstanding temperatures above 70 °C. In fact, NMR data collection was facilitated by our ability to protect the recombinant photoreceptors against contaminating *E. coli* proteases simply by heating the preparations to 65 °C before use. These "sterilized" preparations were surprisingly stable both in terms of solubility and photochemistry, and easily survived long term three-dimensional data collection. This thermostability was also reflected by its Pr → Pfr photoconversion and Pfr → Pr dark reversion kinetics, which are both faster at high temperatures. Taken together, we expect that these Phys rapidly interconvert between Pr and Pfr within the host *Synechococcus* OS-A and OS-B′ organisms when they are grown in their natural daylight environment.

Finally, we show that *SyB*-Cph1(GAF) can be easily labeled isotopically for NMR analyses. By either introducing ^{15}N or ^{13}C isotopes into amino acids or feeding the ^{15}N- or ^{13}C-labeled heme precursor ALA to *SyB*-Cph1(GAF)-expressing cells, we could independently introduce isotopes into the polypeptide and PCB moieties, respectively. The resulting preparations generated two-dimensional NMR spectra with sufficient clarity to discern peaks associated with Pfr from those associated with Pr.

NMR Analysis of the SyB-Cph1 Chromophore PCB—Initial NMR analyses confirmed the utility of *SyB*-Cph1(GAF) preparations for structural studies. One-dimensional NMR spectra of [^{15}N]PCB-labeled preparations in the Pr state detected all four of the pyrrole ring nitrogens (Fig. 8*B*). Surprisingly, only one of these nitrogens (144 ppm) apparently changed its chemical environment after red light irradiation. Collectively, the spectra confirmed RR data that the GAF fragment of *SyB*-Cph1 completes the protonation cycle of the chromophore and implies that the environment/position of three of the four pyrrole N-H groups are similar in the Pr and Pfr states. ^{1}H-^{15}N HSQC spectra both before and after red light irradiation detected only a single ^{1}H-^{15}N chemical shift at 131 ppm, indicating that one of the four bound protons is tightly held and exchanges slowly with the solvent while the remaining three protons readily mix with the surrounding water.

Where are the exchangeable and retained N-H pyrrole-associated protons located in *SyB*-Cph1, and which one of these protons changes its environment upon photoconversion? Prior RR, infrared, and NMR spectroscopic studies with a variety of Phys, including *Synechocystis* Cph1, have suggested that the B and C pyrrole rings move little during photoconversion with most of the movement involving rings A and D (23, 32–34, 62, 71–73). Contrary to the expected large movements of the D-ring following the *Z* to *E* isomerization of the C15–C16 methine linker double bond, it has been proposed further that the A-ring undergoes the more pronounced conformational changes, potentially via a *Z-syn* to *Z-anti* rotation around the C5–C6 methine bridge between rings A and B.

Our ^{15}N and ^{13}C NMR data with *SyB*-Cph1(GAF) are consistent with these interpretations. The high resolution crystal structure of *Dr*BphP assembled with BV showed that the pyrrole nitrogens present in the A–C-rings are held in a *ZZ-syn,syn* configuration as Pr and hydrogen bond with the centrally positioned pyrrole water (see Fig. 8*A*), whereas the D-ring N-H group is contorted 44° out-of-plane in a *Z-anti* configuration and held in place by a second hydrogen bond network involving His-290 and water 2 (13). Assuming this configuration holds true for *SyB*-Cph1 assembled with PCB, we predict that the exchangeable protons (detected at 160, 156, and 144 ppm) are all bound to the A–C-rings. This assignment is consistent with the RR data, which unambiguously show that the pyrrole rings B and C are protonated with the protons rapidly exchanging with the solvent (13). The free exchange of the ring-A–C protons with the solvent is also plausible in view of the deprotonation/protonation cycle of the chromophore during Pr → Pfr photoconversion (18, 19).

Only one of the exchangeable protons in *SyB*-Cph1(GAF) changed environment/location upon photoconversion to Pfr. It appeared in our one-dimensional ^{15}N NMR spectra as a peak at 144 ppm, which diminished in height during red-light irradiation concomitant with the appearance of a new peak at 142 ppm. If we assume that the B- and C-rings are in similar chemical environments and are more rigidly held via their propionate side chains (10, 19), then the moving pyrrole ring is best assigned to the A-ring. In support, Rohmer *et al.* (33) tentatively assigned a similar ^{15}N chemical shift, which moved from 146.8 to 142.8 ppm during photoconversion, to the A-ring nitrogen of *Synechocystis* Cph1(PAS-GAF-PHY) fragment.

The remaining slowly exchangeable proton nitrogen in *SyB*-Cph1(GAF), which had a cross-peak at 131 ppm (^{15}N chemical shift), would then be assigned by default to the D-ring pyrrole N-H group (in agreement with Ref. 33). The absence of additional H-N cross-peaks in our ^{1}H-^{15}N HSQC Pr/Pfr spectra overlay further implies that the amide of this ring does not change upon photoconversion (see Fig. 8*C*, *inset*). Why we failed to detect the expected movement of the D-ring by NMR spectroscopy is unclear. It could reflect a role for the PHY domain in stabilizing D-ring in the Pfr conformer and/or the possibility that the *Z* to *E* isomerization does not dramatically affect the environment of the D-ring N-H group in *SyB*-Cph1.

Examination of *SyB*-Cph1(GAF) bearing [^{13}C]PCB by ^{1}H-^{13}C HSQC detected all six predicted methyl groups, and revealed that four of the six experience a different environment after red light irradiation (Fig. 8*C*). Such movements closely parallel those obtained by Strauss *et al.* (32) with *Syn*-Cph1(PAS-GAF-PHY), who showed that all but one of the six methyl groups acquire alternate peaks after red light saturation. The peak of one methyl in particular (15.5 ppm) for *SyB*-Cph1(GAF) moved a considerable distance during photoconversion, implying that it encounters a radically different chemical environment as Pfr. An interesting possibility is that this moving methyl group (like the moving nitrogen) is also associated with the A-ring.

SyB-Cph1(GAF) Is Amenable to ^{1}H-^{15}N-^{13}C Three-dimensional NMR—Although several studies have demonstrated that various regions of the Phy polypeptide move during Pr → Pfr phototransformation (25–31), their exact motions remain to be determined. The small size and thermostability of the *SyB*-Cph1(GAF) truncation coupled with its ability to effectively complete the Pr → Pfr photocycle strongly suggests that this species may help resolve movements in the GAF domain by NMR approaches. Toward this objective we have found that *SyB*-Cph1(GAF) generates excellent three-dimensional NMR spectra using preparations incorporating ^{15}N and ^{13}C into the chromophore or polypeptide. Overlays of either ^{1}H-^{15}N or ^{1}H-^{13}C HSQC spectra from ^{15}N-^{13}C-labeled *SyB*-Cph1(GAF) samples obtained before and during continuous saturating red light irradiations identified numerous new reversible peaks (Fig. 9 and data not shown). These new peaks presumably reflect changing chemical environments of specific amino acid-associated amides during Pr → Pfr photoconversion. Moreover, many of these peaks remained well defined as Pfr, indicating that the corresponding amides now occupy new and stable environments in this state. Clearly, the large number of unique Pfr peaks implies that the GAF domain by itself undergoes a more robust conformational change during phototransformation than we anticipated. Based on these preliminary data, solving the solution structures of both the Pr and Pfr states of the *SyB*-Cph1(GAF) chromoprotein may be within reach.

Potential Use of SyB-Cph1(GAF) Chromoproteins as Fluorophores—Our discovery of a set of *SyB*-Cph1 mutants that emit red fluorescence may have utility in various cell biological and molecular assays as small portable fluorescent tags. In particular, the *SyB*-Cph1(GAF-PHY D86H) mutant emits strong fluorescence and when directly compared was significantly brighter than the previously reported Y176H mutant generated with the PAS-GAF-PHY fragments of *Synechocystis* Cph1 (Fig. 6) (17, 52). The D86H mutant retains its red fluorescence in a monomeric truncation that encompasses only the 200-amino acid GAF domain, thus making this fluorophore even smaller than the commonly used green fluorescent protein (GFP) (70). Potential advantages over other fluorophores such as GFP include the following: (i) its remarkable thermostability, (ii) the large separation of the electronically excited state (Soret transition at 380 nm) from the emitting state (650 nm), which would minimize light contamination, and (iii) the ability to modify fluorescence in both time and space by controlling PCB availability (74). The D86H mutant may also be excited in the first electronic transition with orange light to produce an identical emission peak (data not shown), thus circumventing potential damages/effects induced by UV or blue light excitation. Expression vectors that exploit *SyB*-Cph1(GAF D86H) as a fluorescent reporter either by itself or when fused to other proteins are currently under development.

Acknowledgments—We thank Dr. J. Clark Lagarias for providing the Syn-Cph1(PAS-GAF-PHY) construction in the pBAD-C expression plasmid and for the pL-PCB plasmid that encodes the enzymes needed to synthesize PCB, Dr. Mario Rivera for providing the ^{13}C-isotopically labeled ALA, and Dr. Claudia Cornilescu for help interpreting the NMR spectra. This study made use of the National Magnetic Resonance Facility at Madison, WI, which is supported by National Institutes of Health Grants P41RR02301 (BRTP/NCRR) and P41GM66326 (NIGMS). Additional equipment was purchased with funds from the University of Wisconsin, Madison, National Institutes of Health Grants RR02781 and RR08438, National Science Foundation Grants DMB-8415048, OIA-9977486, and BIR-9214394, and the U. S. Department of Agriculture.

REFERENCES

1. Quail, P. H. (2002) *Nat. Rev. Mol. Cell Biol.* **3,** 85–93
2. Rockwell, N. C., Su, Y. S., and Lagarias, J. C. (2006) *Annu. Rev. Plant. Biol.* **57,** 837–858
3. Vierstra, R. D., and Karniol, B. (2005) in *Handbook of Photosensory Receptors* (Briggs, W. R., and Spudich, J. L., eds) pp. 171–196, Wiley-VCH Press, Weinheim, Germany
4. Smith, H. (1995) *Annu. Rev. Plant Physiol. Plant Mol. Biol.* **46,** 269–315
5. Karniol, B., and Vierstra, R. D. (2003) *Proc. Natl. Acad. Sci. U. S. A.* **100,** 2807–2812
6. Giraud, E., Fardoux, J., Fourrier, N., Hannibal, L., Genty, B., Bouyer, P., Dreyfus, B., and Vermeglio, A. (2002) *Nature* **417,** 202–205
7. Giraud, E., Zappa, S., Vuillet, L., Adriano, J. M., Hannibal, L., Fardoux, J., Berthomieu, C., Bouyer, P., Pignol, D., and Vermeglio, A. (2005) *J. Biol. Chem.* **280,** 32389–32397
8. Bhoo, S. H., Davis, S. J., Walker, J., Karniol, B., and Vierstra, R. D. (2001) *Nature* **414,** 776–779
9. Lamparter, T., Michael, N., Caspani, O., Miyata, T., Shirai, K., and Inomata, K. (2003) *J. Biol. Chem.* **278,** 33786–33792
10. Wagner, J. R., Brunzelle, J. S., Forest, K. T., and Vierstra, R. D. (2005) *Nature* **438,** 325–331
11. Lamparter, T., Mittmann, F., Gärtner, W., Börner, T., Hartmann, E., and Hughes, J. (1997) *Proc. Natl. Acad. Sci. U. S. A.* **94,** 11792–11797
12. Yeh, K. C., Wu, S. H., Murphy, J. T., and Lagarias, J. C. (1997) *Science* **277,** 1505–1508
13. Wagner, J. R., Zhang, J., Brunzelle, J. S., Vierstra, R. D., and Forest, K. T. (2007) *J. Biol. Chem.* **282,** 12298–12309
14. Wu, S. H., and Lagarias, J. C. (2000) *Biochemistry* **39,** 13487–13495
15. Karniol, B., Wagner, J. R., Walker, J. M., and Vierstra, R. D. (2005) *Biochem. J.* **392,** 103–116
16. Hahn, J., Strauss, H. M., Landgraf, F. T., Gimenez, H. F., Lochnit, G., Schmieder, P., and Hughes, J. (2006) *FEBS J.* **273,** 1415–1429
17. Fischer, A. J., and Lagarias, J. C. (2004) *Proc. Natl. Acad. Sci. U. S. A.* **101,** 17334–17339
18. von Stetten, D., Seibeck, S., Michael, N., Scheerer, P., Mroginski, M. A., Murgida, D. H., Krauss, N., Heyn, M. P., Hildebrandt, P., Borucki, B., and Lamparter, T. (2007) *J. Biol. Chem.* **282,** 2116–2123
19. Wagner, J. R., Zhang, Z., von Stetten, D., Gunter, M., Murgida, D. H., Mroginski, M. A., Walker, J. M., Forest, K. T., Hildebrandt, P., and Vierstra, R. D. (2008) *J. Biol. Chem.* **283,** 12212–12226
20. Rüdiger, W., Thümmler, F., Cmiel, E., and Schneider, S. (1983) *Proc. Natl. Acad. Sci. U. S. A.* **80,** 6244–6248

21. Mizutani, Y., Tokutomi, S., and Kitagawa, T. (1994) *Biochemistry* **33,** 153–158
22. Andel, F., III, Lagarias, J. C., and Mathies, R. A. (1996) *Biochemistry* **35,** 15997–16008
23. Foerstendorf, H., Benda, C., Gärtner, W., Storf, M., Scheer, H., and Siebert, F. (2001) *Biochemistry* **40,** 14952–14959
24. Borucki, B., von Stetten, D., Seibeck, S., Lamparter, T., Michael, N., Mroginski, M. A., Otto, H., Murgida, D. H., Heyn, M. P., and Hildebrandt, P. (2005) *J. Biol. Chem.* **280,** 34358–34364
25. Lagarias, J. C., and Mercurio, F. M. (1985) *J. Biol. Chem.* **260,** 2415–2423
26. Noack, S., Michael, N., Rosen, R., and Lamparter, T. (2007) *Biochemistry* **46,** 4164–4176
27. Grimm, R., Eckerskorn, C., Lottspeich, F., Zenger, C., and Rüdiger, W. (1988) *Planta* **174,** 396–401
28. Quail, P. H. (1997) *Plant Cell Environ.* **20,** 657–665
29. Lapko, V. N., Jiang, X. Y., Smith, D. L., and Song, P. S. (1998) *Biochemistry* **37,** 12526–12535
30. Esteban, B., Carrascal, M., Abian, J., and Lamparter, T. (2005) *Biochemistry* **44,** 450–461
31. Natori, C., Kim, J. I., Bhoo, S. H., Han, Y. J., Hanzawa, H., Furuya, M., and Song, P. S. (2007) *Photochem. Photobiol. Sci.* **6,** 83–89
32. Strauss, H. M., Hughes, J., and Schmieder, P. (2005) *Biochemistry* **44,** 8244–8250
33. Rohmer, T., Strauss, H., Hughes, J., de Groot, H., Gärtner, W., Schmieder, P., and Matysik, J. (2006) *J. Phys. Chem. B.* **110,** 20580–20585
34. Hahn, J., Kuhne, R., and Schmieder, P. (2007) *ChemBioChem* **8,** 2249–2255
35. Yu, H. (1999) *Proc. Natl. Acad. Sci. U. S. A.* **96,** 332–334
36. Riek, R., Wider, G., Pervushin, K., and Wüthrich, K. (1999) *Proc. Natl. Acad. Sci. U. S. A.*, **96,** 4918–4923
37. Ulijasz, A. T., Grenader, A., and Weisblum, B. (1996) *J. Bacteriol.* **178,** 6305–6309
38. Gambetta, G. A., and Lagarias, J. C. (2001) *Proc. Natl. Acad. Sci. U. S. A.* **98,** 10566–10571
39. Wang, L., Elliott, M., and Elliott, T. (1999) *J. Bacteriol.* **181,** 1211–1219
40. Venters, R. A., Calderone, T. L., Spicer, L. D., and Fierke, C. A. (1991) *Biochemistry* **30,** 4491–4494
41. Collins, B. K., Tomanicek, S. J., Lyamicheva, N., Kaiser, M. W., and Mueser, T. C. (2004) *Acta Crystallogr. Sect. D. Biol. Crystallogr.* **60,** 1674–1678
42. Scheer, H. (1984) in *Techniques in Photomorphogenesis* (Smith, H. H., and Holmes, M. G., eds) pp. 227–256, Academic Press, New York
43. Kneip, C., Hildebrandt, P., Schlamann, W., Braslavsky, S. E., Mark, F., and Schaffner, K. (1999) *Biochemistry* **38,** 15185–15192
44. Delaglio, F., Grzesiek, S., Vuister, G. W., Zhu, G., Pfeifer, J., and Bax, A. (1995) *J. Biomol. NMR* **6,** 277–293
45. Allewalt, J. P., Bateson, M. M., Revsbech, N. P., Slack, K., and Ward, D. M. (2006) *Appl. Environ. Microbiol.* **72,** 544–550
46. Bhaya, D., Grossman, A. R., Steunou, A. S., Khuri, N., Cohan, F. M., Hamamura, N., Melendrez, M. C., Bateson, M. M., Ward, D. M., and Heidelberg, J. F. (2007) *ISME J.* **1,** 703–713
47. Park, C. M., Kim, J. I., Yang, S. S., Kang, J. G., Kang, J. H., Shim, J. Y., Chung, Y. H., Park, Y. M., and Song, P. S. (2000) *Biochemistry* **39,** 10840–10847
48. Ishizuka, T., Narikawa, R., Kohchi, T., Katayama, M., and Ikeuchi, M. (2007) *Plant Cell Physiol.* **48,** 1385–1390
49. Bhaya, D., Takahashi, A., and Grossman, A. R. (2001) *Proc. Natl. Acad. Sci. U. S. A.* **98,** 7540–7545
50. Kilian, O., Steunou, A. S., Fazeli, F., Bailey, S., Bhaya, D., and Grossman, A. R. (2007) *Appl. Environ. Microbiol.* **73,** 4268–4278
51. Park, C. M., Shim, J. Y., Yang, S. S., Kang, J. G., Kim, J. I., Luka, Z., and Song, P. S. (2000) *Biochemistry* **39,** 6349–6356
52. Fischer, A. J., Rockwell, N. C., Jang, A. Y., Ernst, L. A., Waggoner, A. S., Duan, Y., Lei, H., and Lagarias, J. C. (2005) *Biochemistry* **44,** 15203–15215
53. Yang, X., Stojkovic, E. M., Kuk, J., and Moffat, K. (2007) *Proc. Natl. Acad. Sci. U. S. A.* **104,** 12571–12576
54. Stock, A. M., Robinson, V. L., and Goudreau, P. N. (2000) *Annu. Rev. Biochem.* **69,** 183–215
55. Wexler, M., Sargent, F., Jack, R. L., Stanley, N. R., Bogsch, E. G., Robinson, C., Berks, B. C., and Palmer, T. (2000) *J. Biol. Chem.* **275,** 16717–16722
56. Davis, S. J., Vener, A. V., and Vierstra, R. D. (1999) *Science* **286,** 2517–2520
57. Strauss, H. M., Schmieder, P., and Hughes, J. (2005) *FEBS Lett.* **579,** 3970–3974
58. Cherry, J. R., Hondred, D., Walker, J. M., Keller, J. M., Hershey, H. P., and Vierstra, R. D. (1993) *Plant Cell* **5,** 565–575
59. Edgerton, M. D., and Jones, A. M. (1992) *Plant Cell* **4,** 161–171
60. Blumenstein, A., Vienken, K., Tasler, R., Purschwitz, J., Veith, D., Frankenberg-Dinkel, N., and Fischer, R. (2005) *Curr. Biol.* **15,** 1833–1838
61. Shlyk-Kerner, O., Samish, I., Kaftan, D., Holland, N., Sai, P. S., Kless, H., and Scherz, A. (2006) *Nature* **442,** 827–830
62. Mroginski, M. A., Murgida, D. H., and Hildebrandt, P. (2007) *Acc. Chem. Res.* **40,** 258–266
63. Murgida, D. H., von Stetten, D., Hildebrandt, P., Schwinte, P., Siebert, F., Sharda, S., Gärtner, W., and Mroginski, M. A. (2007) *Biophys. J.* **93,** 2410–2417
64. Fodor, S. P., Lagarias, J. C., and Mathies, R. A. (1990) *Biochemistry* **29,** 11141–11146
65. Limbach, H. H., Hennig, J., Kendrick, R., and Yannoni, C. S. (1984) *J. Am. Chem. Soc.* **106,** 4059–4060
66. Falk, H. (1989) *The Chemistry of Linear Oligopyrroles and Bile Pigments*, Springer-Verlag, New York
67. Rivera, M., and Walker, F. A. (1995) *Anal. Biochem.* **230,** 295–302
68. Scheerer, P., Michael, N., Park, J. H., Noack, S., Forster, C., Hammam, M. A., Inomata, K., Choe, H. W., Lamparter, T., and Krauss, N. (2006) *J. Struct. Biol.* **153,** 97–102
69. von Stetten, D., Gunther, M., Kaminski, S., Scherer, P., Krauss, N., Lamparter, T., Forest, K. T., Vierstra, R. D., Gärtner, W., Murgida, D. H., Mroginski, M. A., and Hildebrandt, P. (2008) *Angew. Chem.,* in press
70. Li, X., Zhang, G., Ngo, N., Zhao, X., Kain, S. R., and Huang, C. C. (1997) *J. Biol. Chem.* **272,** 28545–28549
71. van Thor, J. J., Mackeen, M., Kuprov, I., Dwek, R. A., and Wormald, M. R. (2006) *Biophys. J.* **91,** 1811–1822
72. Mroginski, M. A., Murgida, D. H., von Stetten, D., Kneip, C., Mark, F., and Hildebrandt, P. (2004) *J. Am. Chem. Soc.* **126,** 16734–16735
73. Inomata, K., Hammam, M. A. S., Kinoshita, H., Murata, Y., Khawn, H., Noack, S., Michael, N., and Lamparter, T. (2005) *J. Biol. Chem.* **280,** 24491–24497
74. Miller, A. E., Fischer, A. J., Laurence, T., Hollars, C. W., Saykally, R. J., Lagarias, J. C., and Huser, T. (2006) *Proc. Natl. Acad. Sci. U. S. A.* **103,** 11136–11141
75. Remberg, A., Lindner, I., Lamparter, T., Hughes, J., Kneip, C., Hildebrandt, P., Braslavsky, S. E., Gärtner, W., and Schaffner, K. (1997) *Biochemistry* **36,** 13389–13395
76. Karniol, B., and Vierstra, R. D. (2004) *J. Bacteriol.* **186,** 445–453